



## **Research on Remote Sensing Applications in Malta**

*Massimo Darmanin*

*Supervisor: Mr Frankie Inguanez*

June, 2022

A dissertation submitted to the Institute of Information and  
Communication Technology in partial fulfillment of the requirements for  
the degree of B.Sc. (Hons.) Software Development

# Dedication

*This research is dedicated to my partner, Francesca, who has been a consistent source of inspiration and support during my graduate school and life problems. I am grateful for your presence in my life.*

*This work is also dedicated to my parents, Anthony and Christine Darmanin, who have always loved me unconditionally and inspired me to work hard for the things I want to achieve by their wonderful example.*

# Acknowledgements

I would like to express my gratitude to my instructor, Mr. Frankie Inguanez, for providing critical feedback and insightful comments throughout my dissertation. Without a question, he was a mentor and an inspiration. Also a thank you for all those who helped by offering me support throughout this thesis. Finally, I have to mention my dog Bianca for all the moral support throughout this academic journey.

## **Abstract**

This research explores the possibility of detecting, observing and analysing the Urban Heat Island Effect over the Maltese islands. The focus of this study was based on the collection of data gathered through remote sensing technologies for the months of March till August of the years 2019, 2020 and 2021. The inclusion of March, April and May came from the idea of observing what happened during the lockdown Malta had experienced during these months of the year 2020. Sentinel-3 remotely sensed data was utilised to conduct research for this project. This study produced the Land Surface Temperature(LST) and Normalised Difference Vegetation Index(NDVI) by reprojecting, cloud masking and excluding high LST Uncertainty pixel values via the products obtained from Sentinel-3 using ESA's common architecture for all Sentinel Toolboxes, Snap Desktop. Study areas included the Maltese islands, the main island of Malta and its urban and rural areas. This was achieved by using the contouring option in QGIS which this research was able to focus its area of study to specific parts of Malta. Hence, NDVI was used to look into any possible links between urban and rural LST of Malta. Observations revealed that the UHI effect during summer were more intense than winter, however the predicted shape and usual observations usually associated with inland cities UHI effects were not present. Instead, the UHI in Winter, albeit much less intense, behaves much more like the observations in literature reviewed. These unique observations have been associated with coastal cities. The effect of the sea breeze on temperatures is mitigated by the presence of vast bodies of water, causing local climate change. These observations were backed by that data analysis of each product, which was then split into 2 time periods; Covid period (March, April and May) and Summer period (June, July and August). Each period was composed of multiple products, within the months mentioned, for the years of 2019 till 2021. Analysed data showed an upward trend in LST values and downward trend for NDVI, slowing down in momentum briefly in the year 2020. Moreover, this research looked into the possibility of observing LST and NDVI correlation, which was observed and calculated its correlation coefficient.

# Contents

<b>List of Figures</b> . . . . .	<b>vi</b>
<b>List of Tables</b> . . . . .	<b>viii</b>
<b>Chapter 1: Introduction</b> . . . . .	<b>1</b>
1.1 Motivation . . . . .	1
1.2 Aim . . . . .	2
1.3 Research questions . . . . .	2
1.3.1 Is Remote Sensing a viable option to track and observe the UHI effect in Malta? . . . . .	2
1.3.2 Does the UHI effect exist in Malta? . . . . .	3
1.3.3 Can UHI be tracked and analysed accurately over a period of years using Remote Sensing technologies? . . . . .	3
1.3.4 What kind of observations can this data provide? . . . . .	3
<b>Chapter 2: Literature Review</b> . . . . .	<b>4</b>
2.1 The Urban Area . . . . .	4
2.1.1 Urban Sprawl . . . . .	4
2.2 Study Area . . . . .	5
2.2.1 Climate . . . . .	6
2.2.2 Urbanisation in Malta . . . . .	6
2.3 Urban Heat Island (UHI) . . . . .	7
2.3.1 Effects . . . . .	9
2.4 Satellites, Orbits and Sensors . . . . .	10
2.5 Land cover classification . . . . .	11
2.6 Unsupervised classification . . . . .	12
2.7 Atmospheric Correction . . . . .	12
2.8 Similar Researches involving LST and UHI . . . . .	13
2.8.1 Analysis & Precision . . . . .	13
2.8.2 Detecting UHI . . . . .	15
<b>Chapter 3: Research Methodology</b> . . . . .	<b>19</b>
3.1 Hypothesis . . . . .	19
3.2 Collection of Data . . . . .	21
3.2.1 LST . . . . .	21

3.2.2	NDVI . . . . .	22
3.3	Study Area . . . . .	22
3.4	Preparing the Data . . . . .	23
3.5	Spatial Mapping . . . . .	24
3.5.1	SUHI Surface Urban Heat Island . . . . .	25
<b>Chapter 4 :</b>	<b>Findings &amp; Discussion of Results . . . . .</b>	<b>27</b>
4.1	Data Validation . . . . .	27
4.2	Visualising and observing Data . . . . .	28
4.2.1	Observing LST . . . . .	29
4.2.2	Observing NDVI . . . . .	30
4.2.3	Other Observations . . . . .	31
4.3	Analysing Data . . . . .	32
4.3.1	2019 March - May . . . . .	32
4.3.2	2019 June - August . . . . .	33
4.3.3	2020 March - May . . . . .	34
4.3.4	2020 June - August . . . . .	35
4.3.5	2021 March - May . . . . .	35
4.3.6	2021 June - August . . . . .	36
4.4	Overall Analysis . . . . .	36
4.4.1	2019 March - May — 2021 March - May . . . . .	37
4.4.2	2019 June - August — 2021 June - August . . . . .	37
4.4.3	LST vs NDVI correlation . . . . .	38
<b>Chapter 5 :</b>	<b>Conclusion . . . . .</b>	<b>53</b>
5.1	Overview . . . . .	53
5.2	Limitations and Recommendations . . . . .	56
<b>Chapter A :</b>	<b>. . . . .</b>	<b>58</b>
<b>Bibliography</b>	<b>. . . . .</b>	<b>74</b>

## List of Figures

2.1	Image sourced from land8.com . . . . .	8
2.2	How the Urban Heat Island occurs - image sourced from Yamamoto (2006) . . . . .	10
2.3	Methodology used to analyse the accuracy of LandSat 8 and Sentinel 3 - image sourced from Hidalgo García (2021) . . . . .	15

2.4	Average daily temperatures of both urban and rural locations - image sourced from Kolokotsa et al. (2009) . . . . .	16
2.5	local climatic zones definitions. Source: Hidalgo García & Arco Díaz (2021) . . . . .	17
2.6	Local Climate Zone Classification Mapping and Location of monitoring points. Image source: The National Geographic Institute (Spain's Ministry of Transport), Hidalgo García & Arco Díaz (2021) . . . . .	18
3.1	Methodology used for this research. . . . .	20
3.2	The actual shape files used for this research - image obtained by using QGIS . . . . .	25
3.3	Raster image of NDVI LST from a Sentinel-3 product . . . . .	26
4.1	Overall LST and the weather report data comparison for all periods . . .	27
4.2	Land Cover Map 2020 (Malta) - image sourced from the European Space Agency . . . . .	28
4.3	Mean LST for each of the processed products in bar graph format . . . .	30
4.4	LST visualisation comparing LST values from March with July . . . . .	39
4.5	LST visualisation comparing LST values from March with August . . . .	40
4.6	NDVI and LST visual representation of April 13th 2020 and March 12th 2021, over the Maltese Islands . . . . .	41
4.7	NDVI and LST visual representation of June 9th 2019 over the Maltese Islands . . . . .	42
4.8	LST visual representation of June 5th 2019 and August 2nd over the Maltese Islands . . . . .	43
4.9	LST visual representation of a before and after rain occurred over the Maltese Islands . . . . .	44
4.10	LST visual representation of how cloud masking is rastered whenever there is cloud presence detected . . . . .	45
4.11	A line graph displaying the average Mean LST across March, April and May for 2019 - 2021 for the island of Malta. . . . .	46
4.12	A line graph displaying the average Mean LST across March, April and May for 2019 - 2021 for the Urban and Rural Areas of the Island of Malta. . . . .	46
4.13	A line graph displaying the average Mean NDVI across March, April and May for 2019 - 2021 for the island of Malta. . . . .	47
4.14	A line graph displaying the average Mean NDVI across March, April and May for 2019 - 2021 for the Urban and Rural Areas of the Island of Malta. . . . .	47
4.15	A line graph displaying the average $SUHI_{MEAN}$ and $SUHI_{MAX}$ across March, April and May for 2019 - 2021 for the Urban and Rural Areas of the Island of Malta. . . . .	48
4.16	A line graph displaying the average Mean LST across June, July and August for 2019 - 2021 for the island of Malta. . . . .	48

4.17	A line graph displaying the average Mean LST across June, July and August for 2019 - 2021 for the Urban and Rural Areas of the Island of Malta. . . . .	49
4.18	A line graph displaying the average Mean NDVI across June, July and August for 2019 - 2021 for the island of Malta. . . . .	49
4.19	A line graph displaying the average Mean NDVI across June, July and August for 2019 - 2021 for the Urban and Rural Areas of the Island of Malta. . . . .	50
4.20	A line graph displaying the average $SUHI_{MEAN}$ and $SUHI_{MAX}$ across June, July and August for 2019 - 2021 for the Urban and Rural Areas of the Island of Malta. . . . .	50
4.21	Mean LST processed in Line graph format across all periods . . . . .	51
4.22	Mean NDVI processed in Line graph format across all periods . . . . .	51
4.23	A bar graph displaying the correlation coefficient between Mean LST and Mean NDVI all periods studied . . . . .	52
A.1	March - May Averages for Mean LST . . . . .	58
A.2	March - May Averages for Mean NDVI . . . . .	58
A.3	March - May Averages for $SUHI_{MEAN}$ and $SUHI_{MAX}$ . . . . .	58
A.4	June - August Averages for Mean LST . . . . .	59
A.5	June - August Averages for Mean NDVI . . . . .	59
A.6	June - August Averages for $SUHI_{MEAN}$ and $SUHI_{MAX}$ . . . . .	59
A.7	Overall average Mean LST of Malta for all periods . . . . .	59
A.8	Overall average Mean LST of the Urban and Rural areas for all periods . . . . .	60
A.9	Overall average Mean NDVI of Malta for all periods . . . . .	60
A.10	Overall average Mean NDVI of the Urban and Rural areas for all periods . . . . .	61
A.11	Overall average $SUHI_{MEAN}$ and $SUHI_{MAX}$ of the Urban and Rural areas for all periods . . . . .	61

## List of Tables

A.1	Mean and Max LST for all products used for the study area of Malta(island) pt.1 . . . . .	62
A.2	Mean and Max LST for all products used for the study area of Malta(island) pt.2 . . . . .	63
A.3	Mean LST for all products used for The Urban and Rural Area pt.1 . . . . .	64
A.4	Mean LST for all products used for The Urban and Rural Area pt.2 . . . . .	65
A.5	Max LST for all products used for The Urban and Rural Area pt.1 . . . . .	66



A.6	Max LST for all products used for The Urban and Rural Area pt.2 . . .	67
A.7	Mean NDVI for all products used for Malta, the Urban and Rural Area pt.1	68
A.8	Mean NDVI for all products used for Malta, the Urban and Rural Area pt.2	69
A.9	SUHI_MAX and SUHI_MEAN for all products used for The Urban and Rural Area pt.1 . . . . .	70
A.10	SUHI_MAX and SUHI_MEAN for all products used for The Urban and Rural Area pt.2 . . . . .	71
A.11	Weather Station Report of each product date pt.1 . . . . .	72
A.12	Weather Station Report of each product date pt.2 . . . . .	73

# Chapter 1

## Introduction

Technology has progressed since the humble beginnings of the tiny satellite resurgence in the 1980s to support an ever more accurate sensory readout and data delivered. Prior to the recent economic boom that Malta has seen in the previous years, its leaders rarely saw the need to investigate the possible applications of remote sensing the way bigger, more affluent countries do. Despite the fact that Malta is a small island, with a recent shift in the economy and a diversification of influence from international investments, there is an ever-increasing need to keep up with and extend prospective applications fit for accurately monitoring and surveilling its area.

### 1.1 Motivation

This paper tries to propose a solution to the problem by presenting data and a case study of how remote sensing can help this island. Prior to the Sentinel Missions, publicly available remote sensing satellites were not accurate or precise enough for Malta to be considered a feasible choice. A growing problem currently being faced by the Maltese citizens is the ever encroachment of development in rural areas and the lack of green spaces in the urbanised areas when compared to other foreign countries such as Slovenia, Sweden or Switzerland. Obviously these countries do not suffer from the same constraints our little island has to face. However, by using remote sensing technologies, our

limited resources can be used to their utmost potential, building a better planned future while mitigating and reducing our footprint on the environment and our own health.

## **1.2 Aim**

The main goal of this research is about using readily available remote sensing technologies and find a use case to study and observe over the Maltese Islands. By doing so, this research hopes to look at all the challenges faced throughout the study in order to document, observe and analyse. The Maltese Islands' population growth and economic development have resulted in a rise in the demand for housing and other amenities. These and other causes contributed to the phenomena of urban sprawl, particularly in rural areas. For this reason, UHI (Urban Heat Island effect) has been chosen to be studied and observed. The reason behind observing and analysing UHI instead of other case studies is due to the fact that there is very limited material and awareness on the subject in Malta. Therefore this research's aim is about exploring remote-sensing technologies and how they may benefit our society while also raising awareness about UHI and its impact on society while exploring the possibility of finding any correlation between LST (Land Surface Temperature) and NDVI (Normalised Difference Vegetation Index).

## **1.3 Research questions**

### **1.3.1 Is Remote Sensing a viable option to track and observe the UHI effect in Malta?**

Is remote sensing for Malta a viable option? What remote sensing applications are best suited for Malta? Are these choices dependable? This research will focus on the data extraction and manipulation deriving from remote sensing products, more specifically, the SLSTR Level-2 LST products from the Sentinel-3 mission. By answering this question, this research hopes to shed more insights on the use cases available which can be

done using current remote sensing technologies and their ability to cater to the Maltese geographical situation.

### **1.3.2 Does the UHI effect exist in Malta?**

Does UHI exist in Malta? And if it does exist, to what level does the UHI effect the Maltese landscape? Is it limited to a single area? Does it envelope the whole islands or is it specific to the individual area? What factors are driving the UHI effect?

### **1.3.3 Can UHI be tracked and analysed accurately over a period of years using Remote Sensing technologies?**

If the UHI effect exists in Malta, is it a viable option to use remote sensing products in order to track and analyse this phenom over a period of years? Is the data being used reliable and accurate? Are there any external factors to look into when using remote sensing products for such a case study?

### **1.3.4 What kind of observations can this data provide?**

What kind of data does remote sensing products offer? Can this data be manipulated with other metrics or indexes in order to produce extra relevant data? What are the limitations of this data? What can we learn as a society from the observations produced and analysed?

# Chapter 2

## Literature Review

### 2.1 The Urban Area

Urban areas, also referred to as built-up areas, are human settlements with high population densities and infrastructures of the built areas. Urbanisation creates urban areas, and these are usually categorised by the urban morphology such as cities, towns or suburbs. Five key parameters were used in the UNICEF report of 2021<sup>1</sup> to characterise an urban area: administrative criteria or political boundaries, the existence of urban characteristics, economic drive, population density and a threshold population size (Pacione 2009). The threshold population size for an urban settlement is generally around 2,000 residents, however, this number varies from 200 to 50,000 people<sup>2</sup>. This means that the figure which defines an urban area may differ from one place to another.

#### 2.1.1 Urban Sprawl

The first recorded word “sprawl” was used by Earle Draperone, who was one of the earliest city planners in the South Eastern side of the United States of America in the late 1930s (Nechyba & Walsh 2004). However, the phrase “urban sprawl” has been defined in many different ways. According to Bhatta et al. (2010), this is due to the fact

---

<sup>1</sup><https://www.unicef.org/media/84881/file/SOWC-2012-executive-summary.pdf>

<sup>2</sup><https://ourworldindata.org/urbanization>

that Urban sprawling is a phenomenon which can be viewed from different perspectives. As a result, the definition of urban sprawl is very ambiguous, which is why researchers opt for solely discussing term without applying their own definition (Bhatta et al. 2010).

A number of key features keep reappearing whenever urban sprawling is mentioned in texts. Most of them mention fragmentation, decentralisation, loss of space and density features (Torrens 2008). Galster et al. (2001) analysed social science and planning literature and suggested that definitions of urban sprawl are to be categorised into six general groups, which are:

1. The embodiment of the characteristics of sprawl such as Los Angeles.
2. The aesthetic judgement about a general pattern of the urban development.
3. The cause of an externality such as the isolation of the poor in the inner city, relying heavily on motor vehicles, destruction and loss of environmental qualities and the spatial discrepancy between jobs and housing.
4. The result or effect of an independent variable such as poor planning, fragmentation in the local governance, or exclusionary zoning.
5. The existing pattern of development such as distance to central facilities, leapfrogging, dispersion of employment, residential development and continuous strip development.
6. The development of that of which occurs over a period of time as an urban area expands outwards.

## **2.2 Study Area**

Malta is an archipelago in the centre area of the Mediterranean sea, about 80km south of Italy. Only the three largest islands are inhabited. These islands, Malta, Gozo and Comino consist of numerous bays, which feature landscapes of low hills with terraced fields. The islands have a Mediterranean climate, with mild winters and hot summers.

Even though Malta has no permanent rivers or lakes due to its climate, it does temporally host some type of water bodies such as valleys and ponds during times of high rainfall. Rainfall generally happens during autumn and winter as summer is mostly dry.

### **2.2.1 Climate**

Average yearly temperature is around 23°C during daytime and 15.5°C during nighttime. The coldest month of the year is January with an average temperature of 12.9°C while the warmest month is August, with an average temperature of 27.5°C. Shifts in temperature are rare occurrences for the islands<sup>3</sup>. The approximate number of sunshine hours is around 3000 per annum, averaging from 5.2 hours in December to 12 hours in July. This is important since on average, Malta has double that of cities in the Northern part of Europe<sup>4</sup>.

### **2.2.2 Urbanisation in Malta**

Eurostat describes Malta as being composed of two larger urban areas, which they branded as “Valletta” and “Gozo”. It should be noted that the main urban area covers the entire main island. The European Spatial Planning Observation Network described Malta as a functional urban area (FUA). The Urban sprawl in Malta is always increasing since population growth creates the need for more housing units. According to the<sup>5</sup>, since 1998 the percentage of the Maltese Urban population grew from around 91.7% to just below 95% in 2018 and is increasing each year. ESPON and Eu Commission studies stated that, “the whole territory of Malta constitutes a single urban region”. With a population of around 400,000 residents and an area of 3.16 km<sup>2</sup>, Malta is one of the most densely populated countries around the globe<sup>6</sup>.

---

<sup>3</sup><http://meteo-climat-bzh.dyndns.org/listenormale-1991-2020-1-p138.php>

<sup>4</sup><https://web.archive.org/web/20150806124550/http://www.maltaweather.com/information/maltas-climate/>

<sup>5</sup><https://data.worldbank.org/topic/urban-development?end=2018&locations=MT&start=1998>

<sup>6</sup><https://worldpopulationreview.com/countries/malta-population/>

When comparing urban permeation within the 28 European Union and 4 European Free Trade Association countries, Malta scored a very high urban permeation units per square meter value. So high in fact that when combining the total permeation units per square meter value for the aforementioned countries, the result is three times less than that of the Maltese Islands alone, which was 5.5 urban permeation units per square meter<sup>7</sup>. Another study by Melchiorri et al. (2018) shows that 64 countries worldwide surpass the degree of urbanisation and agglomeration, and Malta was one of these countries mentioned.

## **2.3 Urban Heat Island (UHI)**

Research and studies regarding Urbanisation frequently speak of the Urban Heat Island effect due to the fact that it is the biggest threat associated with urbanisation and industrialism (Tan et al. 2009). The Urban Heat Island (UHI) effect, is a heat accumulation phenomenon often characterised by the urban climate created by urban constructions and general human activities (Arnfield 2003, Nakayama & Fujita 2010). According to Oke (1982), Urban Heat Islands have been well studied and documented, however the basic understanding of this topic is very limited. This has changed since further advancements in technology and global warming has been taken into priority in last few years. Starting in the early 19<sup>th</sup> century, a scholar named Luke Howard, was the first person to measure and discuss the UHI effects, during a study about the urban climate in London, England. Following this research, many scholars worldwide started researching on the characteristics of the UHI effect (Yang et al. 2016). These studies observed that there was a significant difference between air temperature recorded at urban areas with those located in rural regions (Landsberg 1981). This affect of urbanisation on long-term temperature records, has also been detected for cities with populations less than 10,000 citizens (Karl et al. 1988).

The very first studies done by the World Meteorological Organisation (1982) and Oke

---

<sup>7</sup><https://www.eea.europa.eu/publications/environmental-indicator-report-2016/download>



## Why the urban heat island effect occurs

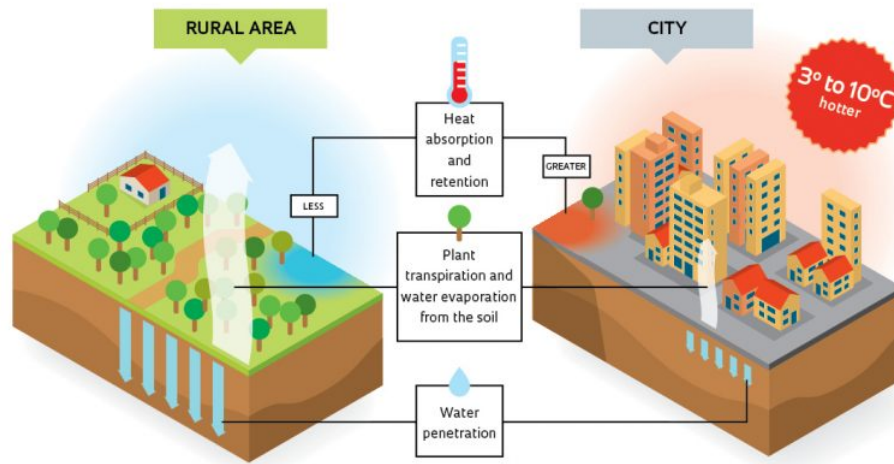


Figure 2.1: Image sourced from land8.com

(1982) showed that UHI effect has the potential of increasing air temperature in a city by around 2°C and 8°C. That said, more recent studies using more accurate measurements illustrate an increase in temperature by 5°C and 15°C (Santamouris 2013). UHI stems from the changing nature of our urban cities, the result of a decrease in vegetation, higher prevalence of dark surface and an increase in anthropogenic heat production (Stone et al. 2010). Akbari & Rose (2008) conducted a study on different metropolitan areas in the USA and concluded that knowledge of the urban fabric and surface conditions of our cities is an important aspect to look at in order to explore and research further effects of possible UHI mitigation measures.

The Urban Heat Island can be represented by plotting a curve from one side of the urban city to the other, thus mapping graphically the change in temperature from rural to urban environment and then back again to rural. According to Oke (1982) the 'Island' part would be represented by a big spike in the middle of the graph, which generally copies the outline of the urban structures within the given area and is bound by the cliffs either side that mark the urban and rural boundary. This way, UHI is easier to spot the increased temperature difference.

The biggest difference in air temperature between urban and rural areas is often observed during the night, with differences in surface radiant temperature at around mid-day (Roth et al. 1989). It was noted that in terms of readings, during the day, rural areas give out a higher LST mean than urban areas, both in periods of heat wave and periods of normal environmental conditions. However, results from data readings during the night showed that rural areas had an average mean LST lower than urban areas, regardless of environmental conditions. The decrease in amount of heat stored in the soil and surface structures covered by transpiring vegetation in rural areas, compared to the relatively un-vegetated urban areas, has been cited as a major contributor to the UHI effect (Carlson et al. 1981). There are a number of academic sources that confirm this situation between rural and urban areas, especially during the early hours in the morning and at night, motivated by the solar radiation received during the day (Karakuş 2019, Yang et al. 2019, 2020, CaiyanWu et al. 2019, Lemus-Canovas et al. 2020).

However, a study conducted by Martinelli et al. (2020), partially focusing on coastal cities, concluded that sea breezes, which are most prominent around the coast, can reduce temperatures and affect the UHI's configuration. Three of the four weather stations used in this study were located in an area with a maximum distance from the coast of less than 2 km, and hence are subject to the synergistic effect of sea and land wind, as well as the UHI phenomena. This emphasises the importance of taking non-thermometric factors into account, such as elevation, orientation, or position, as well as population expansion and the types of built environment and land cover (Nouri et al. 2017, Stewart et al. 2014).

### **2.3.1 Effects**

As a side effect, Urban Heat Islands release excessive amounts of pollution and greenhouse gases to the atmosphere (EPA, 2020). Children and elderly are prone to extreme temperatures and heatwaves. UHIs have a tendency to multiply the effects of heatwaves. This leads the UHI to influence the air quality in urbanised areas. Cardelino & Chameides (1990) found that an increase in temperature leads to an increase of chemical reactions that forms ozone. Ozone is a toxic greenhouse gas to humans at ground level. This

leads to a range of respiratory ailments such as asthma (Stone Jr & Rodgers 2001). This means that heat islands are the downfall of quality of life around the urban areas (Tan et al. 2009).

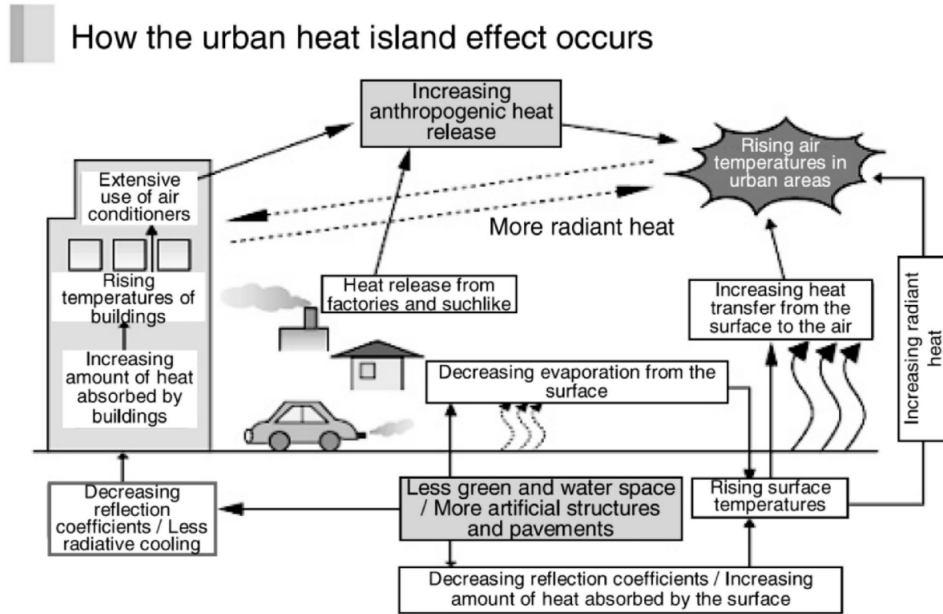


Figure 2.2: How the Urban Heat Island occurs - image sourced from Yamamoto (2006)

## 2.4 Satellites, Orbits and Sensors

The 1990s was a decade in which the use of remote sensing exploded in popularity, using satellite images with TIRS (Thermal Infrared Sensors) to avoid and cut economic costs related to in situ measurements and the scale of operations that bring with them large cities. For the past few decades, various satellite programs have been developed to produce LST products such as Sentinel-3, Modis, EcoStress, Ladis, LandSat8 and various others. The most recent being EcoStress, which was launched into orbit and docked to the ISS (International Space Station) in 2018, Sentinel-3, which comprises of 3 satellite constellation, having the first two satellites launched in 2016 and 2018 respectively, while LandSat 8 launched in 2013. EcoStress, having five TIRS bands and a single shortwave infrared band, provides with LST estimates at a resolution of

70m. Sentinel-3 comes equipped with three TIRS channels, S7-S9 bands, which provide LST estimates with a resolution of 1km. Interestingly, although being the longest in orbit, LandSat 8 features two TIRS bands 10 and 11 which provide LST estimates at a resolution of 100m.

## **2.5 Land cover classification**

Land use classification can be obtained by using data acquired from remote sensing products and process the data by means of image classification. Image classification is the manipulation remote sensing data by applying a set of rules that groups various different pixels in terms of their attributes that split the whole data into sub-categories. These categories are separated by decision boundaries which are then labelled according to the group (Elachi & Van Zyl 2021). By assigning labels according to these groups, users are able to obtain thematic maps (Schowengerdt 1997). As the name suggests, a thematic map is a type of map which focuses on a particular theme that is directly linked to a specific geographic region. Some examples of methods which could be used to classify a multi-spectral remote sensing product are:

1. Unsupervised classification
2. Supervised classification
3. Non-parametric statistics
4. Fuzzy classification
5. Crisp classification
6. Per-pixel classification
7. Object-based classification

(Jensen 1986).

## 2.6 Unsupervised classification

Unsupervised image classification is the process where each image in a given data-set is pointed out as a member of one of the fundamental categories which are present in the image collection without the need of using labelled training samples. The unsupervised grouping of images depend on unsupervised machine learning algorithms for its implementation (Olaode et al. 2014). Clustering used for unsupervised classification is one of most used methods for processing data from remote sensing data of the planet Earth (Jensen 1996).

## 2.7 Atmospheric Correction

Atmospheric correction in remote-sensing is the removal of scattering and absorption effects coming from the atmosphere to obtain the surface properties. Prior reaching the sensor of the satellite, EM (Electro-Magnetic) radiation passes through the atmosphere twice. Irradiance is the downwelling (short-wave) radiation from the sun while radiance is the upwelling (long-wave) radiation from Earth to the sensor. Absorption however reduces the intensity with a haziness effect, making EM energy to scatter and redirects it in the atmosphere, leading to an adjacent effect where pixels close-by are shared <sup>8</sup>. This radiation-atmosphere interaction notably interferes with the multi-spectral sensors aboard remote-sensing satellites, especially data used for monitoring. As an example, land-use observations experience wave-length scattering as the radiation goes through the atmosphere (Bian et al. 2018). Knowing this, Hadjimitsis et al. (2010) noted that it is the key to plan about potential impacts on the quality of the data. By knowing such interactions, appropriate atmospheric correction is applied during the pre-processing part of the satellite data.

The sensor aboard the satellite records both the obvious reflected brightness coming from the object and also records the brightness of the atmosphere in tandem. This means that the value of any given pixel recorded is not the actual radiance reflecting from the

---

<sup>8</sup>[gisgeography.com/atmospheric-correction](https://gisgeography.com/atmospheric-correction)

object (Tyagi & Bhosle 2014). Hence the main point of atmospheric correction is to quantify both properties of the pixel value obtained. This is due to the fact that the value of each aspect catalogued by the sensor is not known. However, when the value of each property is recorded via atmospheric correction, the study can be done with the appropriate radiance values (Hadjimitsis et al. 2010).

There are plenty of implementations of atmospheric correction (Ilori et al. 2019), such as the Top of Atmosphere(TOA) correction, which is used in this study. These implementations are split into two types; Absolute and Relative correction methods (Mahiny & Turner 2007). The main difference between these methods is that the Absolute methods convert the Digital Number(DN) value to either surface reflection or surface radiance, while the Relative methods do not include the true reflectance due to the absence of a solid base of physics (Yu et al. 2010). Furthermore, the absolute atmospheric correction implementations lessens the scattering and absorption process. This happens due to gases and aerosols in the atmosphere. While the Relative implementations reduce the effects of the atmosphere and the effects of the directionality that happens on the surface. These effects of directionality result from the angle at which the sun is facing Earth. Hence, the Relative implementations decrease scatter and other effects (Caselles & Lopez Garcia 1989). As a side note, absolute methods are split into another two additional types. These are the absolute methods which rely on physics and transfer radiation and those Absolute methods which rely only on Images (Yu et al. 2010).

## **2.8 Similar Researches involving LST and UHI**

### **2.8.1 Analysis & Precision**

One of the key parameters needed for the physical processes involving Earth's surface is LST (Zhan et al. 2013). Apart from being essential in temperature-related researches and studies, new methods and techniques for accurately determining LST has become vital for evaluating the exchange in energy and water with the atmosphere (Yu et al. 2014) for various research fields (Cheng et al. 2009, Valor & Caselles 1996, Wan &

Dozier 1996) such as Heat Waves (Jiang et al. 2019, Li & Bou-Zeid 2013, Ramamurthy & Bou-Zeid 2017), and most importantly for this research, Urban Heat Island in urban environments (Barbieri et al. 2018, Keeratikasikorn & Bonafoni 2018, Khalaf 2018, Macarof & Statescu 2017, Sekertekin 2019)

A study conducted by Hidalgo García (2021), looked into the precision of such Split-windows algorithm (SWA) methods using LandSat 8 and Sentinel 3 images in estimating the LST over the city of Granada in Spain. In this study, the choice of Sentinel-3 and LandSat 8 came down to the conclusion based on the relatively recent launch in orbit, since being the least in orbit means that their thermal bands are the least studied to date. Even though EcoStress has been launched in 2018, NASA did in fact warn of anomalies involving the primary storage unit, which has halted the ability of gathering scientific data for some time intervals. In order to determine the accuracy of these LST products, data was validated with the temperature values gathered from in situ, making use of high precision temperature and humidity probes. These probes were strategically placed around Grenada based on the different types of land cover established in the Corine Land Cover inventory (2020), these are:

1. Rural areas
2. Industrial areas
3. Suburban areas
4. Urban areas
5. Urban green areas

With the aid of statistical analysis, the correlation between the data obtained was determined, comparing the data source with seasonal and seasonal variations in the same city.

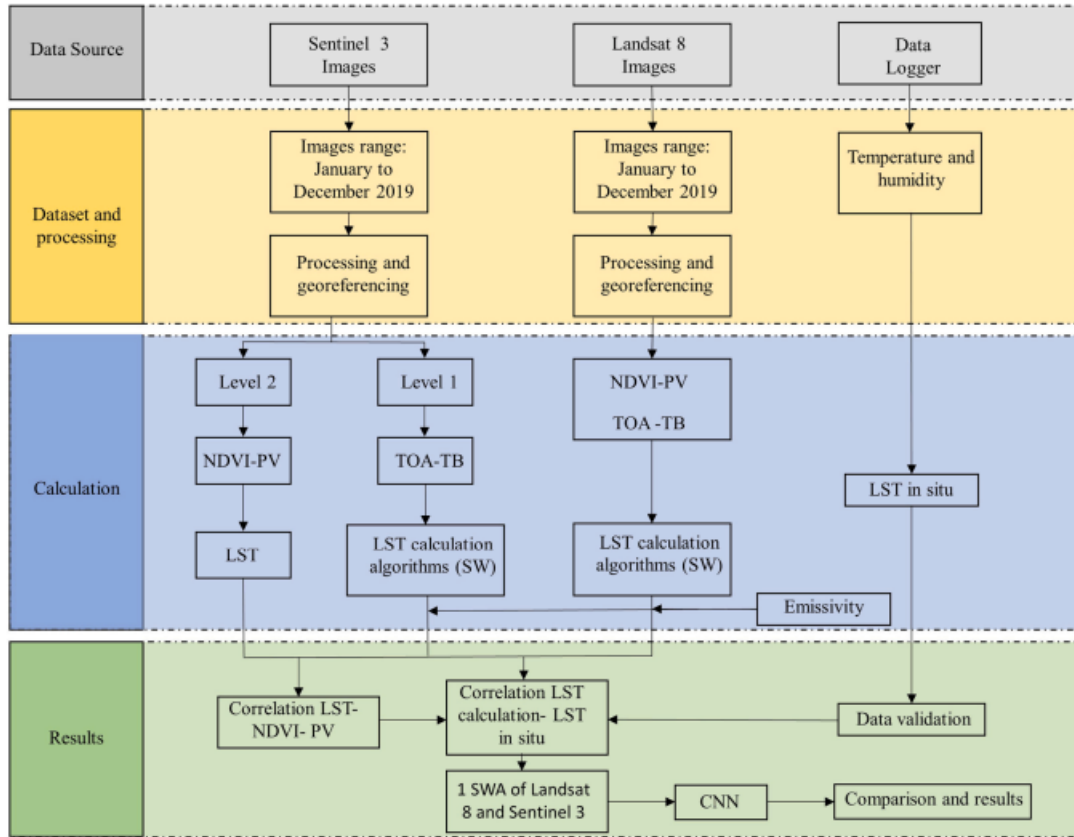


Figure 2.3: Methodology used to analyse the accuracy of LandSat 8 and Sentinel 3 - image sourced from Hidalgo García (2021)

## 2.8.2 Detecting UHI

A study conducted in Crete, a Mediterranean island boasting a climate similar to the Maltese islands, investigated the UHI of a coastal town surrounded by the Aegean sea called Hania (Kolokotsa et al. 2009), accounting for 4,444.1 inhabitants/km<sup>2</sup> making it even more relevant to this study since Malta is also densely populated. From May 26, 2007 to October 24, 2007, temperature and relative humidity readings were taken using nine urban stations and three rural stations, totalling eight data loggers. Simultaneously, meteorological data for the town of Hania was collected and elaborated, including wind speed and direction, barometric pressure, sunlight, and precipitation which were used for cross-correlation with the appearance of the urban heat island (UHI) phenomena (Kolokotsa et al. 2009). As stated by this case study, the highest temperatures



were observed inside the city as compared to the sub-urban areas. The relative humidity was also reported as being lowest in the city centre and highest along the coastlines. This demonstrates that there was a shortage of relative humidity throughout the city. As shown in (Fig 3.2), the largest temperature difference happened on August 25, 2007, with an 8°C difference, while the smallest temperature difference occurred on July 31, 2007, with a 0.6°C difference . The total average temperature for the entire measurement was 2.6°C (Kolokotsa et al. 2009).

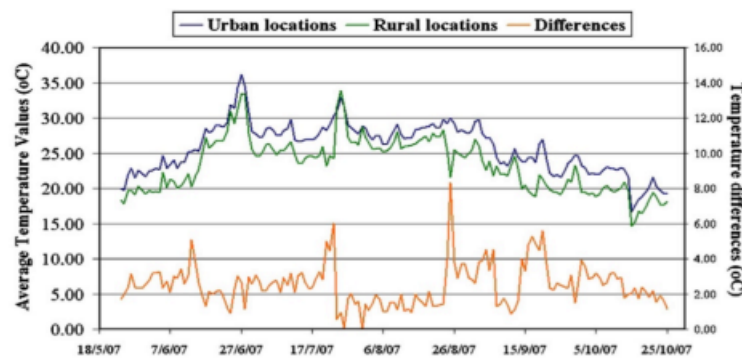





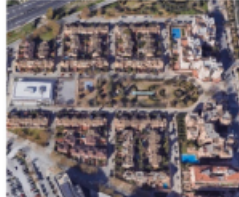
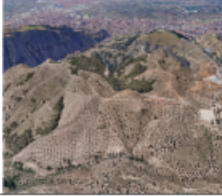

Figure 2.4: Average daily temperatures of both urban and rural locations - image sourced from Kolokotsa et al. (2009)

Furthermore, according to this case study, the intensity of UHI is at its highest towards the start of summer (i.e. June) and gradually declines after September. The largest temperature difference for this measurement occurred in July, presumably indicating that the UHI intensity is at its peak in regions with a Mediterranean climate during this month of the year. Something interesting to note is that the Hania region is rather arid. It barely rains, but when it does, the impact of rainfall in this area is significant. Temperatures resulted in a significant drop in the severity of the UHI in the region (Kolokotsa et al. 2009). As a result, one technique to alleviate the UHI is through precipitation.

In another research by Hidalgo García & Arco Díaz (2021), the city of Grenada was split into six different local climatic zones (LCZ): Compact vs Open High-Rise, Compact vs Open Low-Rise, Scattered Trees and Low Plants.

This was done as an approach to characterise the landscape, making it possible to

Building types and zones.

Built Types	Definition	Built Types	Definition
a) Compact High Rise		b) Compact Low Rise	
	Dense mix of tall buildings to tens of stories. Few or no trees. Land cover mostly paved. Concrete, steel, stone, and glass construction materials.		Dense mix of low-rise buildings (1–3 stories). Few or no trees. Land cover mostly paved. Stone, brick, tile, and concrete construction materials.
c) Open High Rise		d) Open Low Rise	
	Open arrangement of tall buildings to tens of stories. Abundance of pervious land cover (low plants, scattered trees). Concrete, steel, stone, and glass construction materials.		Open arrangement of low-rise buildings (1–3 stories). Abundance of pervious land cover (low plants, scattered trees). Wood, brick, stone, tile, and concrete construction materials.
e) Scattered Trees		f) Low Plants	
	Lightly wooded landscape of deciduous and/or evergreen trees. Land cover mostly pervious (low plants). Zone function is natural forest, tree cultivation, or urban park.		Featureless landscape of grass or herbaceous plants/crops. Few or no trees. Zone function is natural grassland, agriculture, or urban park.

Images source: Google Earth.

Figure 2.5: local climatic zones definitions. Source: Hidalgo García & Arco Díaz (2021)

precisely identify the factors that have the most or least impact on each LCZ. In their research they also established a number of factors: Normalised Difference Vegetation Index (NDVI), Normalised Difference Built-Up (NDBI), Fraction Vegetation Cover (PV), Solar Radiation, Pollution, Impervious Surface Fraction Factor (ISA), Mean of Building Height Factor, Fraction of Building Facades, Number of Vehicles as a Factor, Wind, Altitude and Population Density. With these factors established, the correlation between the data gathered and the relationship between the independent and dependent variables of each LCZ was determined by using Panel Data method, a method of statistical analysis.

Using the strategy used in this research, Hidalgo García & Arco Díaz (2021) were able to represent the probable variances of each LCZ's conditions in the final results, making it a unique and strong approach. This is a particularly useful method for calculating UHI in a medium-sized city with strong thermal contrast and pollution (like

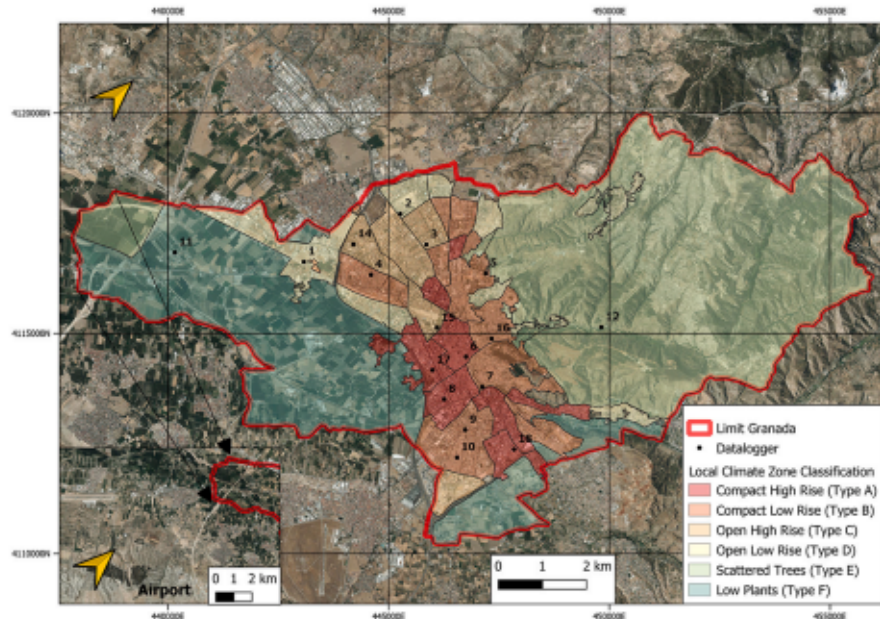


Figure 2.6: Local Climate Zone Classification Mapping and Location of monitoring points. Image source: The National Geographic Institute (Spain's Ministry of Transport), Hidalgo García & Arco Díaz (2021)

Granada does), because it allows one to calculate both daytime and nighttime UHI based on the physical and environmental parameters of each LCZ.

Another research by Sobrino & Irakulis (2020), mentioned that there have been plenty of authors who have written about obtaining LST and urban heat islands on a spectral, temporal and spatial scale and the respective satellite sensors most suitable for SUHI (Surface Urban Heat Island) detection. But all of them focus on a single city or urban agglomeration, where the definition for rural and urban areas was adapted for each study case which makes the job of comparison between cities around the world somewhat of a complication. So instead Sobrino & Irakulis (2020) proposed a new methodology on how to calculate and compare SUHI values generated from urban agglomerations internationally. Their method suggests calculating SUHI for three surrounding areas using only LST acquired during night-time. In their research, this method was applied to 71 selected urban agglomerations around the world.

# Chapter 3

## Research Methodology

The main objective of this research is to use remote sensing technology in order to study and observe UHI on the Maltese Island. Temperature and vegetation have long been studied using Normalised Difference Vegetation Index (NDVI), most of these studies even suggest that NDVI and LST complement each other and have an interrelationship (Guo et al. 2012). Therefore, in order to study and observe UHI, this research will look at the level of vegetation and the land surface temperatures, as done by García (2021).

### 3.1 Hypothesis

While remote sensing has come a long way since its inception, there are still some significant challenges to monitoring a small island in comparison to huge areas and characteristics seen elsewhere in the world. This problem might cause some issues when assessing in detail the Maltese landscape, since spatial resolution has always been the biggest challenge for the Maltese case study. However, this paper is very confident in being able to track and analyse the UHI effect in Malta, albeit with some challenging issues that other bigger study cases never have to experience. Since the recent Covid pandemic, the recent lockdown that the country experienced, could prove to hold some interesting data about how the UHI behaves and therefore shed more insights about un-

derstanding UHI in Malta. The main drawback of remote sensing is cloud coverage. This is not really an issue when studying the summer season, however it might prove challenging when observing the second quarter of the year. This research is expecting to find the UHI effect in Malta, especially in the most dense Urbanised areas. It is also expecting very high LST values and low NDVI values during Summer. On the contrary, since March, April, and May are considered wet months and therefore more vegetation is around the landscape, NDVI values are expected to be higher while LST to be much lower than Summer values. Since the Urban area is part of the coast line, lower than expected LST values are to be expected.

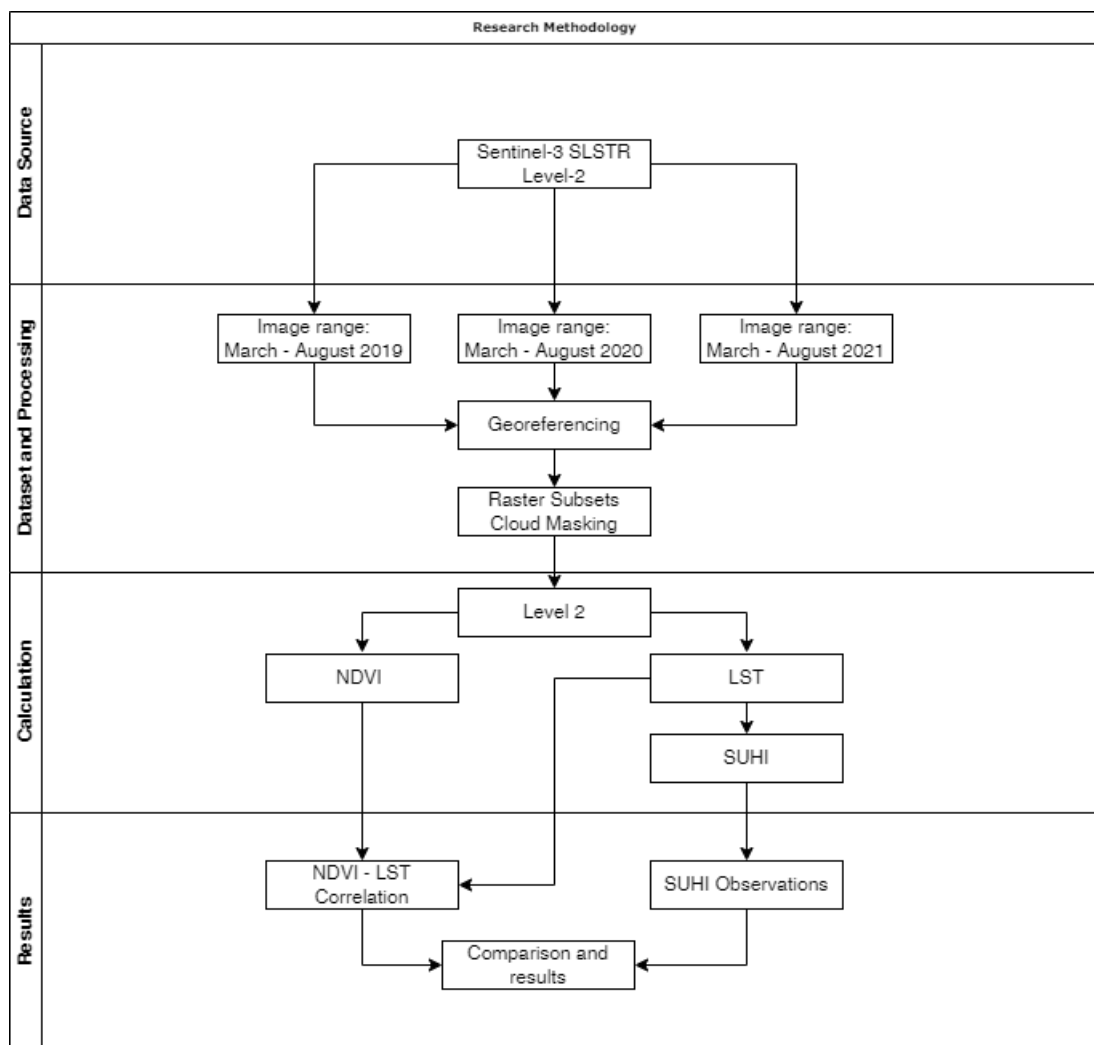


Figure 3.1: Methodology used for this research.

## 3.2 Collection of Data

Remote-sensing Satellites are a great tool for gathering and processing data related to LST. For this research, night-time remote-sensed products have been used, following the suggestions and observations of previously mentioned literature (Karakuş 2019, Hu et al. 2020, Yang et al. 2020). 74 SLSTR Level-2 LST products were gathered from the Sentinel-3 mission, available free on the Copernicus database over the months of March till August, from 2019 up until 2021<sup>1</sup>. Apart from being able to produce both night-time and day-time products, Sentinel-3 also features an NDVI band which shall be used in conjunction with the LST values recorded. Most often, literature focuses on the extreme periods of the year such as the extreme heat of summer. However, given the recent events of the pandemic and its ensuing effects on society, for this research, the months of March till May will be used to observe UHI pre-pandemic, during pandemic and post-pandemic while using the months from June till August to better observe UHI and its growing presence on the Maltese Islands.

### 3.2.1 LST

The SLSTR Level-2 LST products that were used for this research feature land surface data generated on a 1km measurement grid which contains LST values that are computed and stored for each orphan or re-gridded pixel. Indexed across and along track dimensions are the Measurement Dataset (MD)<sup>2</sup>. This data set is processed using a split-window method, which use two different radiances from two channels. This is done to effectively determine the radiometric temperature of the Earth's surface. An algorithm is used for LST which is based on the radiative transfer theory which compare radiation between atmosphere and surface. This algorithm for LST can be stated as:

$$LST = a_0 + b_0T_{11} + c_0T_{12} \quad (3.1)$$

---

<sup>1</sup><https://scihub.copernicus.eu>

<sup>2</sup><https://sentinels.copernicus.eu/web/sentinel/user-guides/sentinel-3-slstr/product-types/level-2-lst>

In this context;  $a_0$ ,  $b_0$  and  $c_0$  are coefficients which rely on land surface emissivity ,atmospheric water vapour and satellite viewing angle. While  $T_{11}$  and  $T_{12}$  represents the brightness temperatures measured at 11  $\mu\text{m}$  and 12  $\mu\text{m}$  respectively<sup>3</sup>.

### 3.2.2 NDVI

Most academic research regarding UHI involves the use of NDVI. NDVI or Normalised Difference Vegetation is used as an indicator of vegetation health present in a given area. Therefore, correlation between vegetation and LST can be calculated. NDVI data was taken from the NDVI band available directly from the data products provided by Copernicus. NDVI is calculated using the following formula:

$$NDVI = \frac{NIR - Red}{NIR + Red} \quad (3.2)$$

## 3.3 Study Area

The major hurdle in estimating  $SUHI_{MEAN}$  and  $SUHI_{MAX}$  is the difficulty in defining the urban area and its surrounding references since there is no clear definition in literature which explains how to select these areas (Sobrino & Irakulis 2020). The study area, consisting of the Maltese archipelago, was mapped using QGIS, an open-source geographic information application, which was used to assign geo-spatial vector data format. This was done by utilising the “New Shape File layer” function from QGIS, which exports the drawn polygon as a shapefile (.shp). This geo-spatial data is used to focus on specific areas, which shall be described later, of the previously downloaded data from the Copernicus database. Since the relative size of the islands and Eurostat describing Malta as being made up of two larger urban areas, “Valletta” and “Gozo”, it was decided that for this research, the main island of Malta would be split into two areas, the East side of Malta counting as the urban area while using the West of Malta as its rural area. Urban

---

<sup>3</sup><https://sentinels.copernicus.eu/web/sentinel/technical-guides/sentinel-3-slstr/level-2/lst-processing>

reference classification was sourced from the free land cover products produced by the European Space Agency Climate Change Initiative <sup>4</sup>.

### 3.4 Preparing the Data

Prior manipulating the product for extracting and visualising data, each product had to be re-projected to the Coordinate Reference System (CRS) EPSG:4326 using ESA's common architecture for all Sentinel Toolboxes, Snap Desktop. CRS is a coordinate-based global, regional or local system which is used to pinpoint geographical entities. CRS is used to define specific map projections while also allowing for transformations between two spatial reference systems. This allowed for the shape files created previously, to create data frames from the areas of interest while also being able to find the relevant pixel data according to location. Since the months of March and April result in mostly cloudy or rainy days, cloud masking had to be applied to the products. The basic idea of this approach is to detect clouds and cloud shadows by using the difference reflectance values between clear pixels and cloud and cloud shadow contaminated pixels, therefore eliminating abnormal values from the final data set. Ghent et al. (2019) describes the algorithm behind LST Uncertainty as a confront to the enormous challenge of using sensitive hardware from orbit, which as a minimum, distinguishes and quantifies between: locally correlated, large-scale systematic and random components should employ a consistent algorithm and a consistent approach to uncertainty analysis. Therefore for this study, any data that the algorithm flagged as having anything greater than 0.2 uncertainty. Cloud masking and the removal of 1st uncertainty of 0.2 was left out from the data set by setting an expression in the LST and NDVI band properties. This was achieved by using the Snap Desktop built in "Batch Processing" feature and by running a graph consisting of a Read, Reproject, Subset and Write functions. By supplying the path location of the previously downloaded products, the Read function opens the products in their raw format. The reprojection function batch processed all

---

<sup>4</sup><https://maps.elie.ucl.ac.be/CCI/viewer/>



of the products into EPSG:4326-WGS84. However, certain products which contained all of the data gathered in a single orbit, proved to take a considerable amount of time when reprojecting the image. Therefore, a Subset function was introduced which crops the image to a particular set of polygon coordinates. Although the Subset function was placed after the Reprojection function, it still functioned as intended and focused on reprojecting that subset rather than the whole orbit, thus reducing processing times. The Write function was used to convert the image produced from its original format into a GEOTIFF, which will be used later on in this research.

### **3.5 Spatial Mapping**

SNAP consists of several toolboxes, some of which can be configured to work on Python by using the “Snappy” interface. By making use of snappy, large volumes of satellite data was efficiently analysed by automating the image processing tasks using python scripts. Metadata of each product, such as satellite name, date and time of recording was extracted and stored in the initial data frame, building an index of products and basic description. Each product was then split into multiple subsets using the previous shape files created for the study areas, focusing on the Maltese main island, the urban area and the rural area individually. Each subset is made up of two Raster bands LST and NDVI.

Null value for SLSTR Level-2 LST products is -32768. These values were removed, cleaning the data from the subsets. After cleaning the data values for LST and NDVI bands, new band data were created which were populated with pixel values and re-shaped for each subset. Although not required, LST values were converted from the original Kelvin metric units to Celsius by subtracting 273.15 from their value. Values were normalised while mean, minimum and maximum pixel values were recorded for each subset. By using the libraries available from matplotlib, it was possible to generate a raster image from each subset. Both NDVI and LST raster interpolation was set to 'nearest', while the colour maps for LST and NDVI were set to cm.jet and cm.RdYlGn respectively.

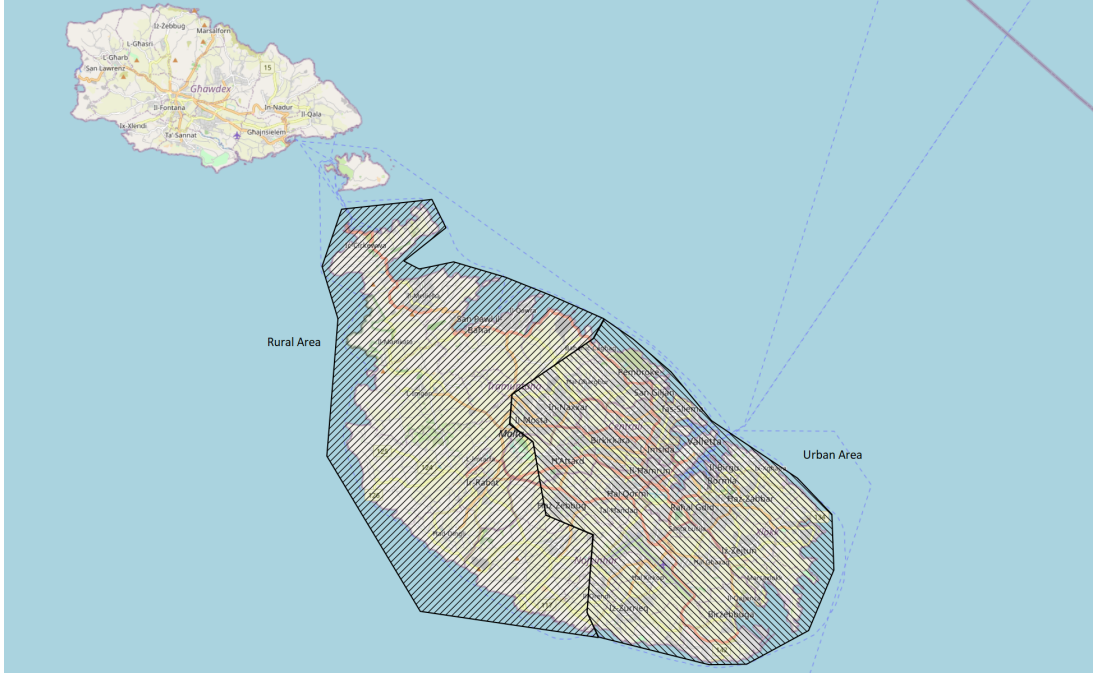


Figure 3.2: The actual shape files used for this research - image obtained by using QGIS

### 3.5.1 SUHI Surface Urban Heat Island

By following Sobrino & Irakulis (2020) methodology and using the night-time obtained LST,  $SUHI_{MAX}$  and  $SUHI_{MEAN}$ , which can be described as thermal differences between the maximum and mean LST of the urban area and the LST surrounding area respectively, can be estimated by using this expression:

$$SUHI_{MAX} = LST_{URB-MAX} - LST_{SUR} \quad (3.3)$$

$$SUHI_{MEAN} = LST_{URB-MEAN} - LST_{SUR} \quad (3.4)$$

The definition for  $LST_{URB-MAX}$  can be defined as the maximum LST (hottest pixel) of the urban area.  $LST_{URB-MEAN}$  refers to the average temperature of the pixels defining the urban area, while  $LST_{SUR}$  can be described as the average temperature of the composing pixels in the surrounding area.

Data recorded from the products were saved to a Comma Separated Values(CSV) file

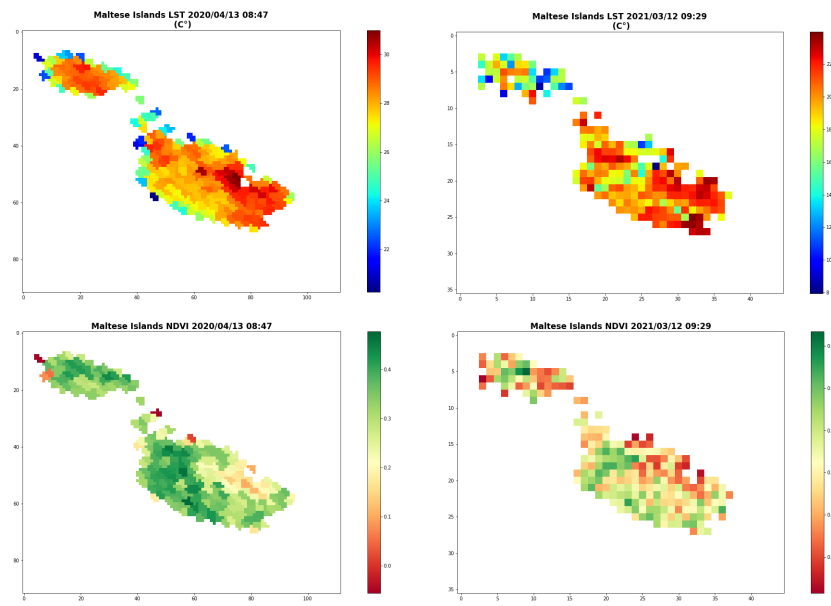


Figure 3.3: Raster image of NDVI LST from a Sentinel-3 product

which shall be used for generating statistical data.

# Chapter 4

## Findings & Discussion of Results

### 4.1 Data Validation

Pérez-Planells et al. (2021) concluded that for the three examined surfaces combined, the operational Sentinel-3A SLSTR LST product is accurate for nighttime data, with an accuracy (systematic uncertainty, i.e., median) of 1.0 K and a precision (random uncertainty, i.e., RSD) of 1.0 K. Therefore, since this research will focus on nighttime data, rigorous data validation will not be part of this chapter. However, for every product downloaded, weather station data has been logged, averaged and compared and referred to LST values throughout this chapter in order to better understand the results at hand.

Period	Temperature (°C) AVG	LST_MEAN	Humidity (%) AVG	Wind Speed (km/h) AVG
2019 March - May	16.2	24.85886	74.94285714	16.07142857
2019 June - August	26.71538462	40.99493	60.53076923	12.62307692
2020 March - May	17.14285714	27.2536	75.71428571	15.49285714
2020 June - August	26.16923077	39.36907	66.06153846	13.2
2021 March - May	17.01538462	28.52872	72.13846154	14.23846154
2021 June - August	26.825	40.386	63.625	11.475

Figure 4.1: Overall LST and the weather report data comparison for all periods

## 4.2 Visualising and observing Data

For observation purposes, this section of this research will focus on the Maltese Islands overall, while observing for patterns or visual cues from the raster images and initial report produced prior extracting and analysing data. Data presented in this chapter consists of 74 products ranging from March till August 2019 - 2021. In depth detail about the data gathered will be tackled later on in this chapter. The LST and NDVI heatmaps of the Maltese islands were obtained by following all the requisite steps as mentioned under the the Methodology, Chapter 3 of this research. This part focuses on the observations and analysis of the hotspots created by the UHI effect in Malta and how the towns and cities, mainly situated on the East side of Malta(island), affect the surrounding temperatures of the urban area by using the LST band from Sentinel-3 products. NDVI however shall be visualised solely for the purpose of observing, through out the given periods, how it correlates and affects LST values in the vicinity, its data is collected and used later on in the discussion of this research.

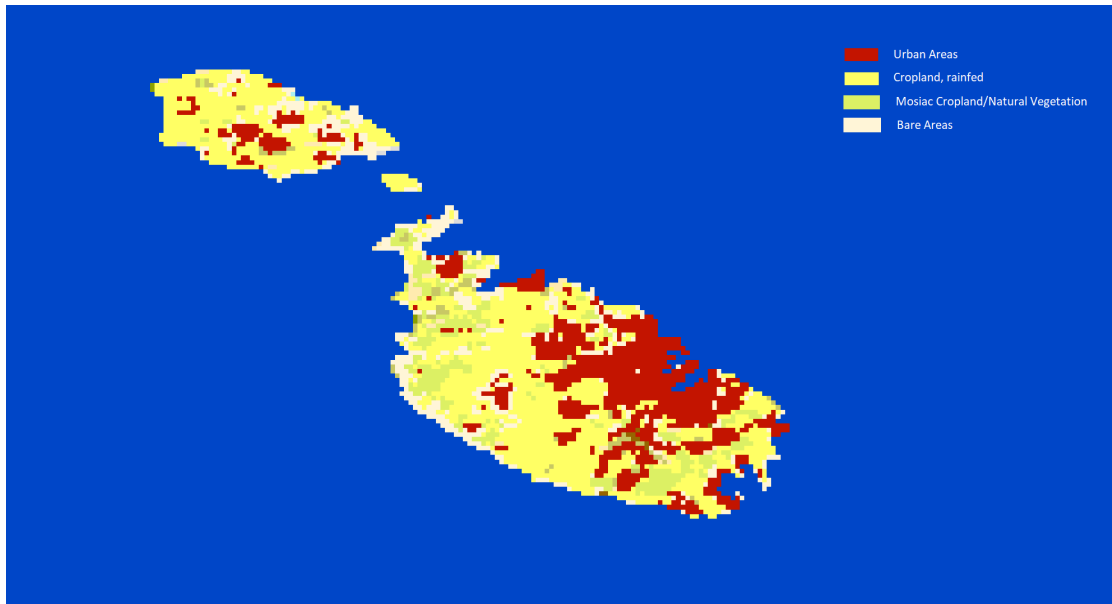


Figure 4.2: Land Cover Map 2020 (Malta) - image sourced from the European Space Agency

### 4.2.1 Observing LST

For the majority of the observations, when LST is compared to Land Cover data, it appears to be following the notion that the UHI effect, is a heat accumulation phenomenon often characterised by the urban climate created by urban constructions and general human activities (Arnfield 2003, Nakayama & Fujita 2010), as it shown in Figure 4.4. It can also be observed the quantity of thermal energy retention, mostly in urban areas, that dot the Maltese landscape, where green spaces and vegetative areas emit the least LST values while developed or barren areas emit the most, acknowledging the observations made by Stone et al. (2010) that UHI comes from the decrease in vegetation, higher prevalence of dark surfaces and the increase in anthropogenic heat production. Referring to Figure 4.4, the notion of Malta being composed of two larger urban areas, “Valletta” and “Gozo” by Eurostat, can be easily validated using the Land Cover data obtained from the European Space Agency Climate Change Initiative program. Therefore, this research assumes “Gozo” and “Valletta” as two separate Urban areas. When comparing “Gozo” with “Valletta”, the first remark that comes from observations is the density of the urban area and its affect on the surrounding area. “Gozo”, having somewhat minimal urbanisation in place, does not “pollute” and affect the surrounding areas as much as “Valletta”. This difference is mostly visible in the Summer period of the year, as peak LST could be seen taking place in areas which are in the surrounding areas of the urban area, with areas such as the south of Malta, where the Maltese Freeport international port station and the Delimara Power Station are located, show the extremities of human interference on a much wider area than usual. Graph 4.3 displays Max LST and Mean LST for the island of Malta for the period of March till August from 2019 till 2021. At around the month of June each year, a noticeable spike in LST occurs. This observation can be linked to the fact that LST peaks during the beginning of summer (in June) and progressively drops after September. The largest temperature difference for this observation occurred in July, implying that the UHI intensity is at its highest in Mediterranean climate zones during this month (Kolokotsa et al. 2009). Figure 4.4 and Figure 4.5 shows the difference in temperatures between the months of March and

August of 2019 and 2020 in heatmap form. These rastered images can be compared and analysed with the land cover data provided from the ESA, detailing land cover type, see Figure 4.2.

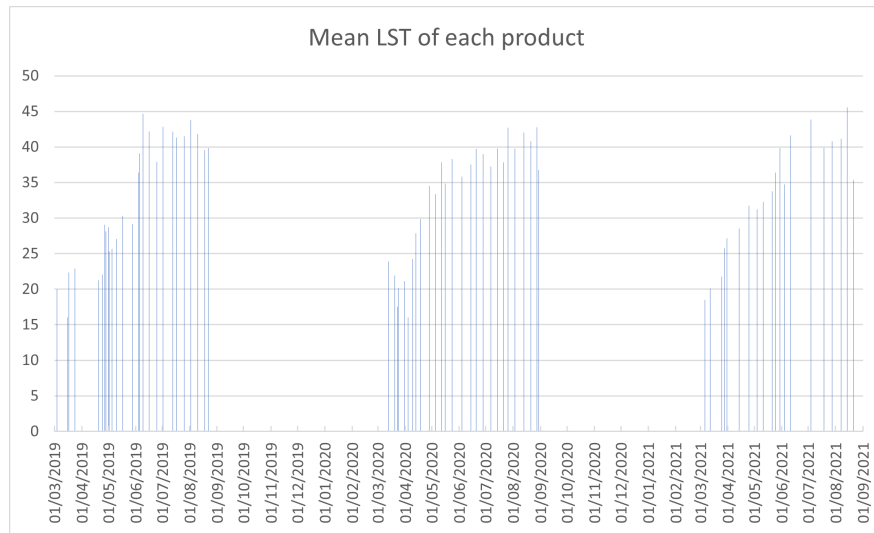


Figure 4.3: Mean LST for each of the processed products in bar graph format

## 4.2.2 Observing NDVI

Temperature and vegetation have long been examined using the Normalised Difference Vegetation Index (NDVI), and many of these research even show that NDVI and LST are complementary and have a link (Guo et al. 2012). Therefore it was the obvious next step in this research to observe and analyse NDVI in relation to LST. By taking advantage of the NDVI band in Sentinel-3, NDVI readings compliment the LST values since they were recorded together on the same orbit. As shown in Figure 4.6 and graph 4.22, using the same reprojected image produced for the LST band, an NDVI raster image is able to give out more details about the underlying contributors to the LST value recorded. NDVI values are set from 0, meaning barren and non-vegetative land, to 1, pointing out to lush vegetative green land. Therefore by comparing data from different periods, NDVI correlation can be observed and validated. The lack of vegetation on the Maltese Island throughout the majority of the year is an alarming observation, as the lack of

green areas contribute to the accumulating rise in surface temperatures created by the UHI effect, hence the extreme LST values recorded in summer periods, which without plant transpiration and water evaporation from the soil, has no way of passively cooling the surrounding area.

### **4.2.3 Other Observations**

Although vegetation and surface types are in fact the main contributors to high LST values, they are not the only driving force in play. As sometimes, LST values do not exactly follow the statements mentioned. Martinelli et al. (2020) mentioned that the creation of the UHI is influenced by the climate and topography of cities, which are mostly governed by their geographical position and that the effect of the sea breeze on temperatures is mitigated by the presence of vast bodies of water, as illustrated in Figure 4.7. This phenomena overlaps with UHI in coastal cities, causing local climate change. Another study conducted in the city of Barcelona (Spain) found that the UHI intensity is weaker in the summer due to the sea breeze effect. As a result, the peak of UHI intensity occurs in December (Salvati et al. 2017). On the other hand, temperature inversions create stable atmospheric zones in the lower atmosphere, resulting in the trapping of pollutants near the ground surface. When the temperature rises with height, or when the potential temperature gradient is positive, this phenomena occurs. Situations like these arise as a result of the ground surface's radiative cooling which results in observing abnormal temperatures in regions or land areas which when following the conventional literature about inland cities says should not exist. An example of such observation is Figure 4.8, where the rural areas had higher LST values than the urban area resting on the coastline. Rainfall has a big impact on UHI. Temperatures in the region led in a dramatic reduction in the severity of the UHI, as mentioned in the research by Kolokotsa et al. (2009), Figure 4.9 compares the visual observable temperature before and after some precipitation occurred.<sup>1</sup>

---

<sup>1</sup><https://weatherspark.com/h/m/150260/2019/5/Historical-Weather-in-May-2019-in-Malta#Sections-Precipitation>



## 4.3 Analysing Data

In this section, this research will focus the study area to the island of Malta. By sub-setting the previous image to focus on one island will give out clearer results as it will focus on just one urban area. As mentioned in the previous chapter, the study area will be further split into two parts; the Urban area and the Rural area. For the scope of this research, Urban Area will be associated with the East of Malta, as there is the bulk of the high density urbanisation on the island, while the West shall be referred to as the Rural Area, accounting for the majority of the green spaces on the island. The data has been grouped and analysed into three-month periods, the “Summer” period and the “Covid” period. Part of this research will look for any abnormalities or deviancy in trend for the period accounting for the lockdown season experienced during the beginning of the pandemic, where most human activities came mostly to a sudden stop. Initial hypothesis stands to understand that some form of noticeable or observable data will come to fruition by studying the before, during and after this event. The “Summer” period however shall be used to analyse peak LST and for comparison between the two periods, as already been observed in the last section. The first part will focus the study area on the whole main island of Malta. In detail discussion of the urban area and rural area will be tackled in the second part of each period.

### 4.3.1 2019 March - May

This period marks a year prior the lockdown season Maltese citizens experienced and as such, this data shall be used as a before human activities stopped briefly and how human activities affect UHI and LST without changing the landscape. Although 2019 is often referred to as the warmest year of a decade<sup>2</sup>, this period is marked as being the coldest period on average when compared to the rest of the periods. The lowest Minimum Average LST for the area of Malta recorded was on the 16th of March 2019, at 16.03°C, being the lowest Minimum LST value of the whole study periods. This is

---

<sup>2</sup><https://www.malteseislandsweather.com/category/reports/annual/>

mostly attributed to the fact that it was recorded after a couple of weeks of heavy dew fall, light rain and thunderstorms. Max Average LST recorded for this period is also the lowest value recorded when compared to the other periods, at 30.3°C while LST median of the whole period is at 25.5°C. Mean LST for the period was at 24.9°C being also the lowest from the set of periods. Mean NDVI for the period is at the highest, with a mean value of 0.29, highest NDVI mean value recorded for the set. Mean LST for the Rural area (West Malta) was at 24.4°C while the Urban area (East Malta) was at 25.3°C. A noticeable difference of 0.9°C between the two areas. Mean NDVI for the Urban Area was recorded at 0.27 while the Rural area was recorded at 0.32.  $SUHI_{MEAN}$  for the period came out to be 0.97°C while  $SUHI_{MAX}$  was at 4.6°C. An interesting point about Figure 4.9 is that between 2nd May and 5th May 2019, rain and cloud coverage cooled down Mean LST for the urban area from 26.22°C to 25.76°C while the rural area increased in Mean LST from 24.18°C to 25.61. This could be the result of the sea breeze effect, which having the Urban area sitting on the coastline can benefit from. As already mentioned indirectly, this period was the hardest to track products which do not have clouds covering the study area. This is reflected in the low LST values recorded over this period, especially for the months of March and April while continuous cloud cover and water precipitation may have contributed to the final analysis of this period. Overall, coldest recorded period and most vegetative with an above average  $SUHI_{MAX}$  and  $SUHI_{MEAN}$ .

### 4.3.2 2019 June - August

This period marks the earliest record of this study towards analysing the extreme temperatures which happen in Summer. Since Summer 2020 was not part of that lockdown season, this period will not be included with the Covid analysis. Summer 2019 marks the period with the lowest average LST of 36.37°C, recorded on the 4th of June 2019. Understandably, the lowest average recorded is at the earliest of the period with temperatures plateauing at the beginning of August, marking a reversal in trend which sees the rest of the month with decreasing LST values. However, the highest Max LST of this

period was in early June, where it peaked at 50.2°C, results conform with the statement that LST peaks during the beginning of summer, around June, and progressively drops after September (Kolokotsa et al. 2009). NDVI values for this period is at a slow steady decline starting at NDVI value 0.25 at the beginning of June and ends the period with a value of 0.21°C, signalling dry season for the most part of the period. Mean LST for the Rural Area was at 40.6°C, while that of the Urban area was 41.9°C, with a difference of 1.3°C it is slightly higher than the difference collected between March and May of 2019.  $SUHI_{MAX}$  was at 5°C while  $SUHI_{MEAN}$  was recorded as 1.3°C. SUHI values for this period were the lowest from the study periods. This could be due to the fact that although  $SUHI_{MAX}$  and  $SUHI_{MEAN}$  were indeed a little lower than usual throughout this period, it was also one of the most stable out of the whole study periods and therefore would not impact the averaged result as much. Mean NDVI levels were both below average when compared to the other periods, with the Urban area having an NDVI value of 0.2 while the Rural area averaged 0.24.

### 4.3.3 2020 March - May

This period marks the year when the lockdown restrictions took place in Malta for the majority of the time frame<sup>3 4</sup>. This means that for a brief moment in history, human activities have halted to running only the essentials, making this an opportunity to study and observe. Although UHI itself is not dependent on ongoing activities, it is still an important contributor which might give some new insights on the subject. Minimum Averaged LST was 16.05°C while the Max LST recorded was 44.58°C. This contrast in extreme LST values when compared to the previous year could be attributed to less rainfall during this period when compared to previous years<sup>5</sup>. On the 23rd and 24th of March 2020, NDVI values recorded had a sudden downward spike and then returns to normal values. Upon further investigation, this turned out to be cloud coverage over

<sup>3</sup><https://www.mondaq.com/human-rights/912314/partial-lockdown-in-malta-to-have-effect-from-2>

<sup>4</sup>[https://www.maltatoday.com.mt/news/national/108479/how\\_covid\\_experts\\_postlockdown\\_plan\\_called\\_for\\_travel\\_ban\\_until\\_september\\_2020#.YpThQKhBwuU](https://www.maltatoday.com.mt/news/national/108479/how_covid_experts_postlockdown_plan_called_for_travel_ban_until_september_2020#.YpThQKhBwuU)

<sup>5</sup><https://www.malteseislandsweather.com/category/reports/annual/>

Malta and the low NDVI reflected as a result of the cloud masking, which nulls the pixel data where clouds are detected as it can be seen in Figure 4.10. However, Mean NDVI value was 0.26, which is equal to the average Mean NDVI value of all “Covid” periods. Average  $SUHI_{MAX}$  was at 4.6°C while  $SUHI_{MEAN}$  was recorded as 0.64°C, a decrease from the previous year. This could be attributed to the unnaturally drier season than usual.

#### **4.3.4 2020 June - August**

During this period, lockdown restrictions were mostly eased or in the works of phasing out. Therefore this period will not be included with the “Covid” period. Minimum average LST and Max averaged LST both were recorded to be cooler than the previous year, with a 35.85°C Minimum LST and a 47°C for Max LST. This makes this years lowest recorded LST by around 0.5°C and a cooler Max LST value difference of 3.2°C than the previous year. Mean LST was at 39.4°C, making it cooler than the previous year. Mean LST over the Rural area was 1.1°C cooler than the Urban area, with values recorded being 39°C for the Rural area and 40.1°C of the Urban area. Mean NDVI showed was as expected, that is NDVI between Rural and Urban areas in summer due to the dryness of the season, difference between the areas is at a minimal. With the Urban area having a mean NDVI value of 0.19 while the Rural area had a 0.22. Average  $SUHI_{MAX}$  was at 4.9°C while  $SUHI_{MEAN}$  was 1.2°C.

#### **4.3.5 2021 March - May**

This period marks a year from the lockdown restrictions. Mean LST for the period was at 28.5°C while Max LST recorded was 47°C, making them the highest average LST value and Max LST recorded value for the “Covid” group. This could be due to the fact that the year 2021 was warmer than usual. The yearly average was exceeded by 1.6 degrees Celsius, with a mean temperature of 19.8 degrees Celsius. Maximum temperatures showed the biggest deviation from the climatic mean. Only the months of

March, April, October, and December had temperatures below the average. Over the course of the year, a number of temperature-related records were broken. On the second weekend of 2021, on Saturday, January 9th, Malta set a new national record for the highest January temperature ever recorded<sup>6</sup>. These are alarming events where the whole climate can be seen to be getting warmer and drier sooner each passing year. However, Mean NDVI value was still at 0.26, the same as the previous year. Average Mean LST over this period for the Rural Area was at 28°C while the Urban Area had a slightly higher average of 29.3°C, the highest from the “Covid” period group. NDVI values in the Urban area showed at 0.24 while in the Rural area it was averaged at 0.28. Average  $SUHI_{MAX}$  was at 4.4°C while  $SUHI_{MEAN}$  was 1.23°C.

#### **4.3.6 2021 June - August**

This is the final period for this study to analyse. The average Mean LST for this period was at 40.4°C while Max LST was 50.1°C, which is noticeably higher than the previous years. Average Mean NDVI was recorded at 0.19, well within average. Mean LST for the Urban Area was 40.9 while in the Rural area it was at 40.1°C. NDVI value for the Rural area was at 0.2 while the urban area was recorded at 0.18.  $SUHI_{MEAN}$  for the period was 0.75°C while  $SUHI_{MAX}$  was at 4.9°C.

### **4.4 Overall Analysis**

This part of the research will focus on the overall results gathered alongside the observations done in the beginning of this chapter. The study periods that will be mentioned are the “Covid” and “Summer” periods. Results are compared and analysed in detail individually depending on the period being discussed.

---

<sup>6</sup><https://www.malteseislandsweather.com/category/reports/annual/>

#### **4.4.1 2019 March - May — 2021 March - May**

Overall, for the “Covid” period, an upward trend in LST values and a downward trend for NDVI was observed. Mean LST increased by 15% going from an averaged LST of 24.86°C in 2019 to 28.53°C in 2021, see Figure 4.11. An interesting point about the study areas is that this increase in temperature is shared equally between the Rural and Urban areas, see Figure 4.12. This means that the Rural area was not able to dissipate heat any quicker than the Urban area. Mean NDVI saw a decrease of 12.4% from 2019 till 2021, see Figure 4.13. However, the decrease in NDVI values in the Rural areas were higher than the Urban Area, with a 13% decrease in the Rural area compared to the 10% decrease in the Urban area, see Figure 4.14.  $SUHI_{MAX}$  saw a decrease of 5% while  $SUHI_{MEAN}$  increased by 26.6%, see Figure 4.15. An interesting point about this period is that a slight decrease in uptrend was noticed throughout the year 2020. This means that daily human activities, although not enough to reverse the uptrend immediately, are also part of the bigger picture when studying UHI.

#### **4.4.2 2019 June - August — 2021 June - August**

For the “Summer” period however, it was the opposite of the “Covid” period. This time frame saw a decrease in Mean LST of 1.5%. Interestingly, mean LST experienced a drop in temperature between Summer 2019 and 2020, as it decreased from 41°C to 39.4°C in 2020. Then in Summer of 2021, temperatures reach almost 2019 levels, at 40.4°C, see Figure 4.16. This downward trend was equal as well between the Rural and Urban areas, having experienced a decrease of 1% and 2% respectively, see Figure 4.17. Mean NDVI however did not see any signs of reversal, as it decreased by 11.4% between 2019 and 2021 and saw no significant changes in the downtrend as visible with LST, see Figure 4.18. Rural areas suffered the most, with a decrease in Mean NDVI of 18.5% decrease compared to the Urban Area’s 14.7% decrease, see Figure 4.19. This downtrend in NDVI could be explained by the increasing development the island is experiencing. Between Spring 2017 and Spring 2019, the vegetation green colour on the islands decreased by

2.45km<sup>2</sup>. This loss could be the result of tree chopping, fewer vegetation, and reduced farming activity while over the course of four years, the Islands' arable and rural areas were degraded by 1.25km<sup>2</sup>, with 0.83km<sup>2</sup> eroded in the past two years. This loss is due to a variety of factors, including increased urbanization and the expansion of urban zones (Zerafa 2020).  $SUHI_{MAX}$  saw a decrease of 2.5% while  $SUHI_{MEAN}$  some what experienced a decrease of 41% from 2019 till 2021. Having decreased from 1.27 to 1.15 between 2019 and 2020, while 2021 came as a surprisingly lower value of 0.75, see Figure 4.20. This value could be result of an anomaly in the data collected on the 21st of August 2021 when  $SUHI_{MEAN}$  was recorded at -1.68 due to a sudden decrease in temperatures between the 14th and the 21st of August, 2021.

#### **4.4.3 LST vs NDVI correlation**

Part of this research includes the exploration of the correlation between LST and NDVI. With the data gathered from all the products, results are as follow; Correlation Coefficient of the main island of Malta is at -0.54, the correlation coefficient of the Rural Area was -0.58 while correlation coefficient of the Urban Area was -0.48, see Figure 4.23. This discrepancy between the Urban and Rural area raise the issue that although LST and NDVI are clearly correlated, there are other factors implicating the effects of NDVI on LST. The most obvious of these factors is the density of water bodies nearby or the water retention available in the air in the form of humidity or dew. Not to mention the inclusion of NDVI and topography of the study area as observed in the beginning of this chapter and mentioned in other literature (Salvati et al. 2017, Martinelli et al. 2020, Kolokotsa et al. 2009).

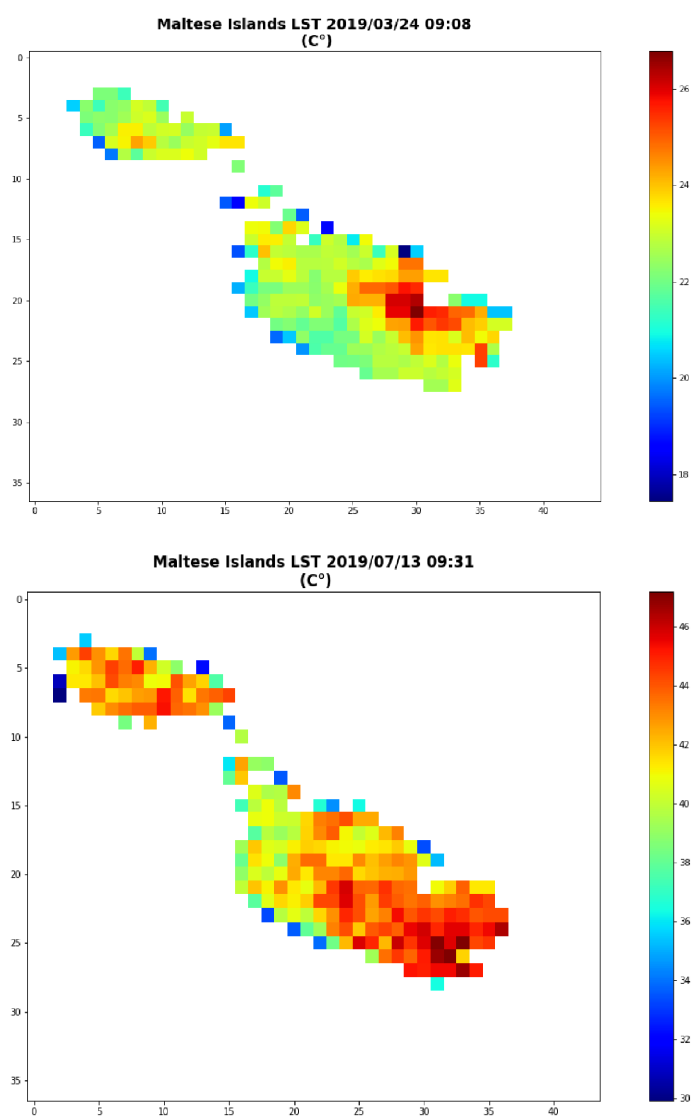


Figure 4.4: LST visualisation comparing LST values from March with July



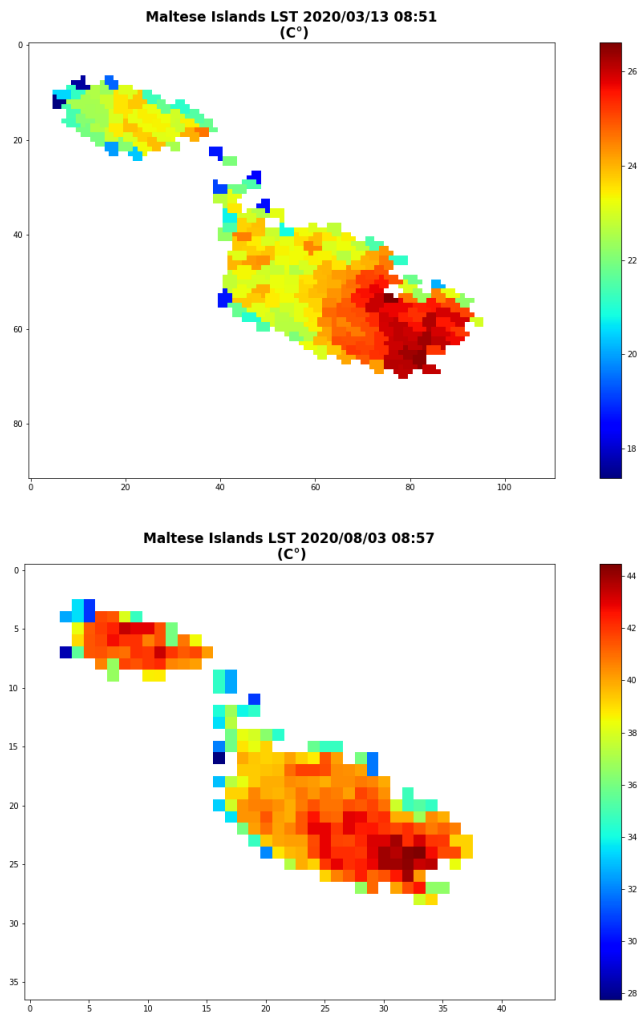


Figure 4.5: LST visualisation comparing LST values from March with August

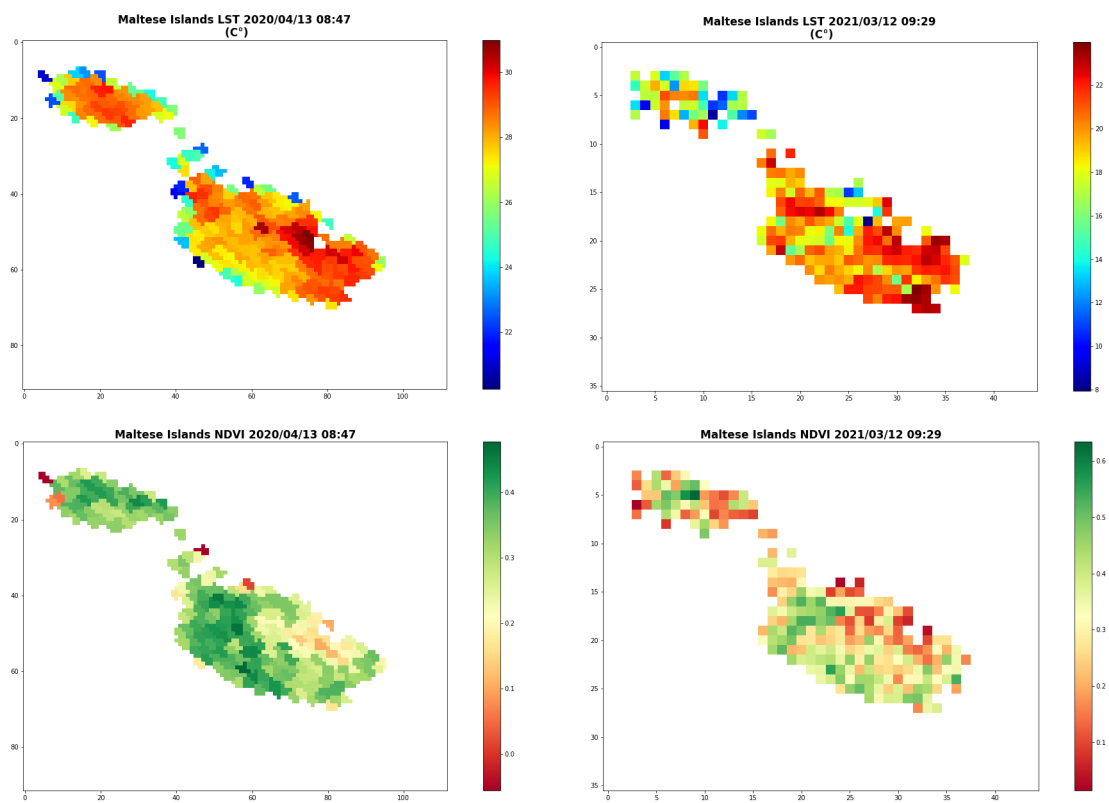


Figure 4.6: NDVI and LST visual representation of April 13th 2020 and March 12th 2021, over the Maltese Islands

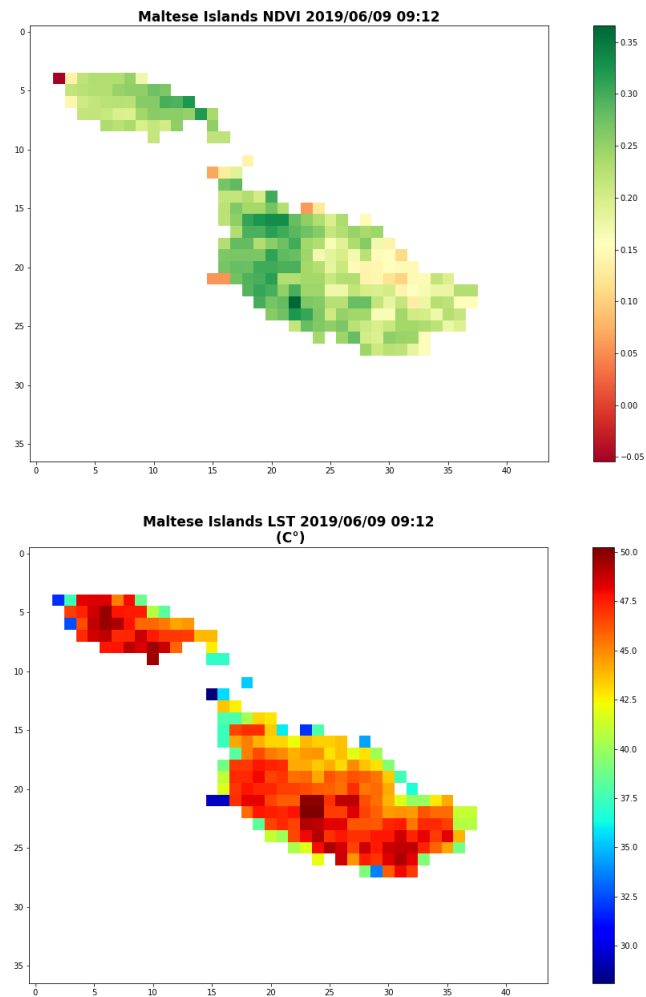


Figure 4.7: NDVI and LST visual representation of June 9th 2019 over the Maltese Islands

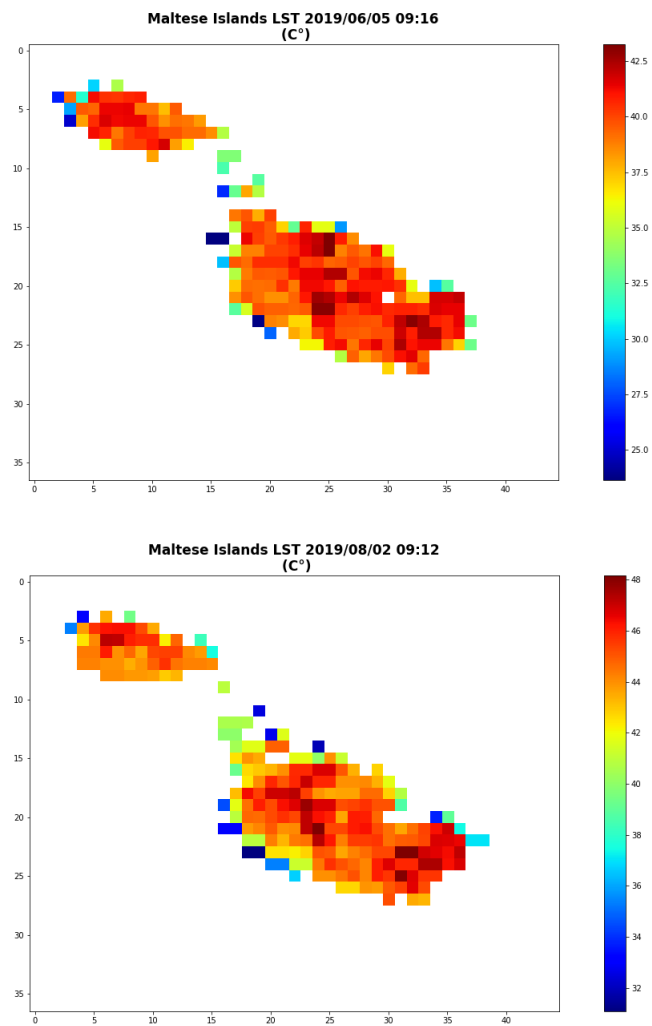


Figure 4.8: LST visual representation of June 5th 2019 and August 2nd over the Maltese Islands

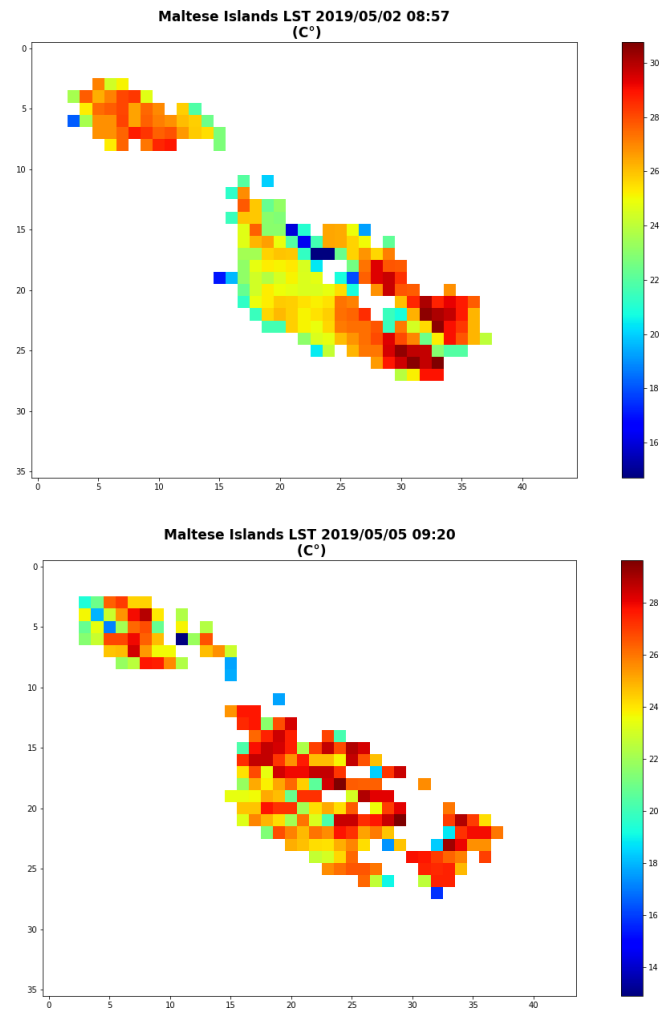


Figure 4.9: LST visual representation of a before and after rain occurred over the Maltese Islands

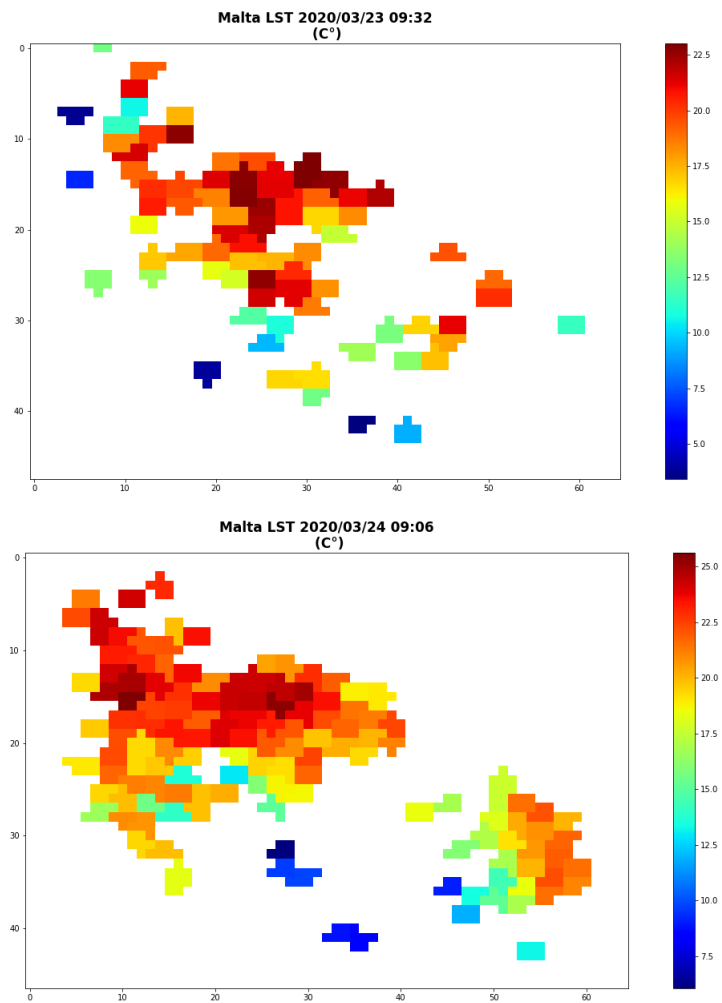


Figure 4.10: LST visual representation of how cloud masking is rastered whenever there is cloud presence detected

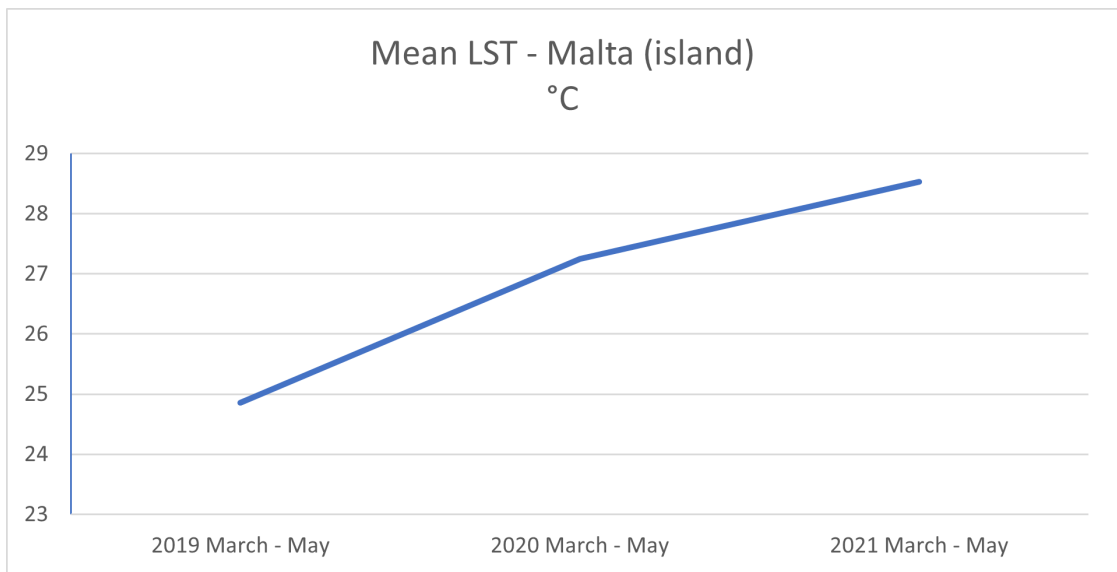


Figure 4.11: A line graph displaying the average Mean LST across March, April and May for 2019 - 2021 for the island of Malta.

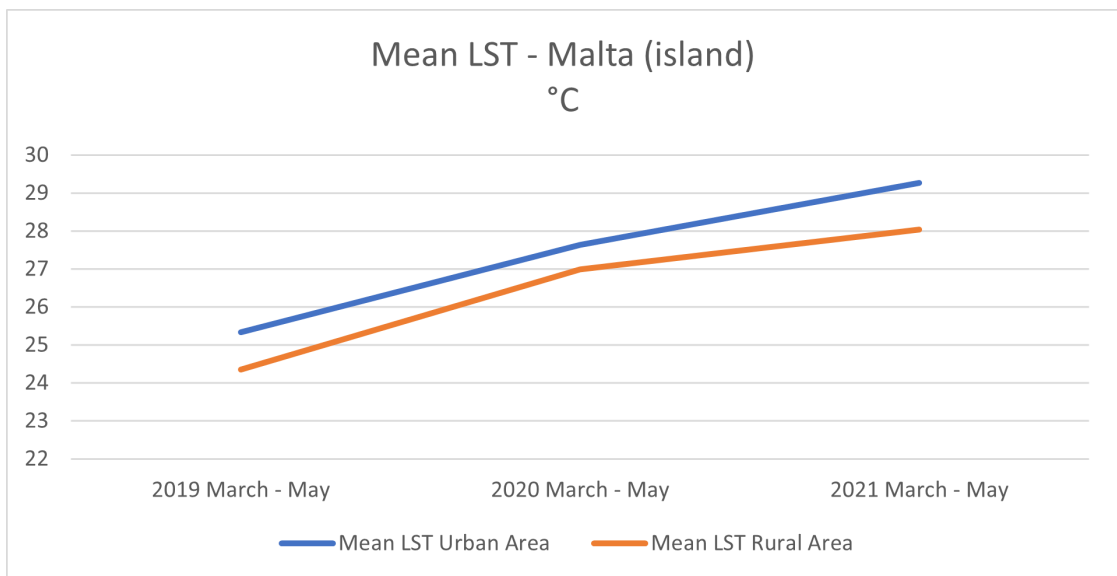


Figure 4.12: A line graph displaying the average Mean LST across March, April and May for 2019 - 2021 for the Urban and Rural Areas of the Island of Malta.

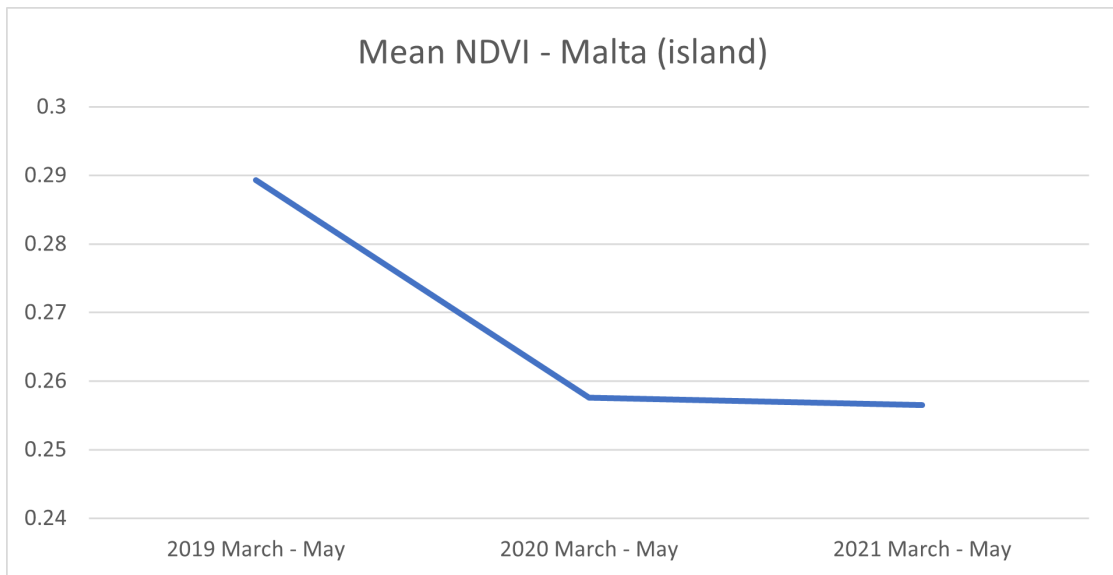


Figure 4.13: A line graph displaying the average Mean NDVI across March, April and May for 2019 - 2021 for the island of Malta.

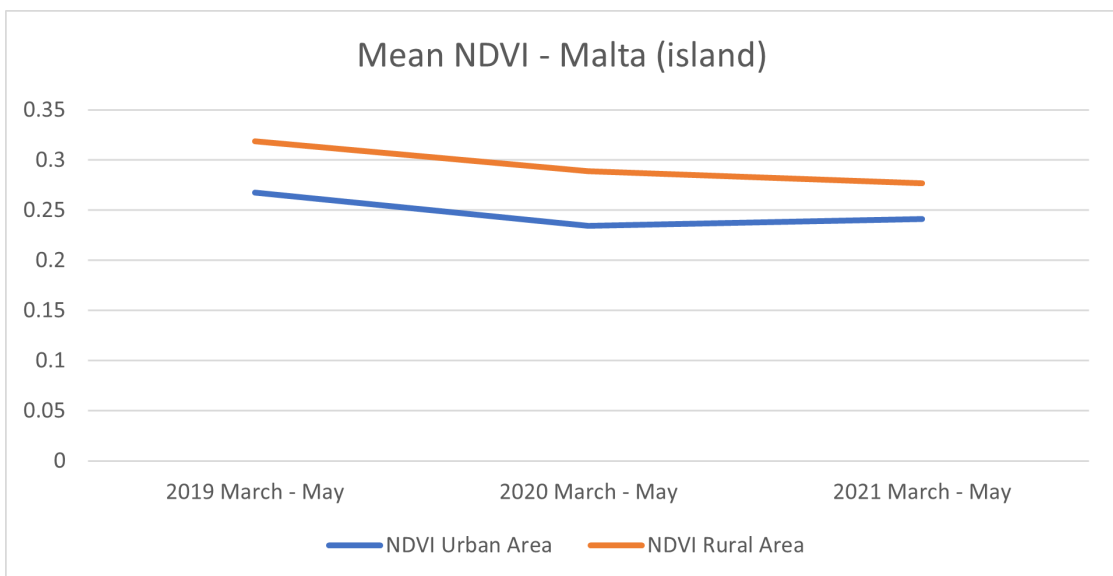


Figure 4.14: A line graph displaying the average Mean NDVI across March, April and May for 2019 - 2021 for the Urban and Rural Areas of the Island of Malta.



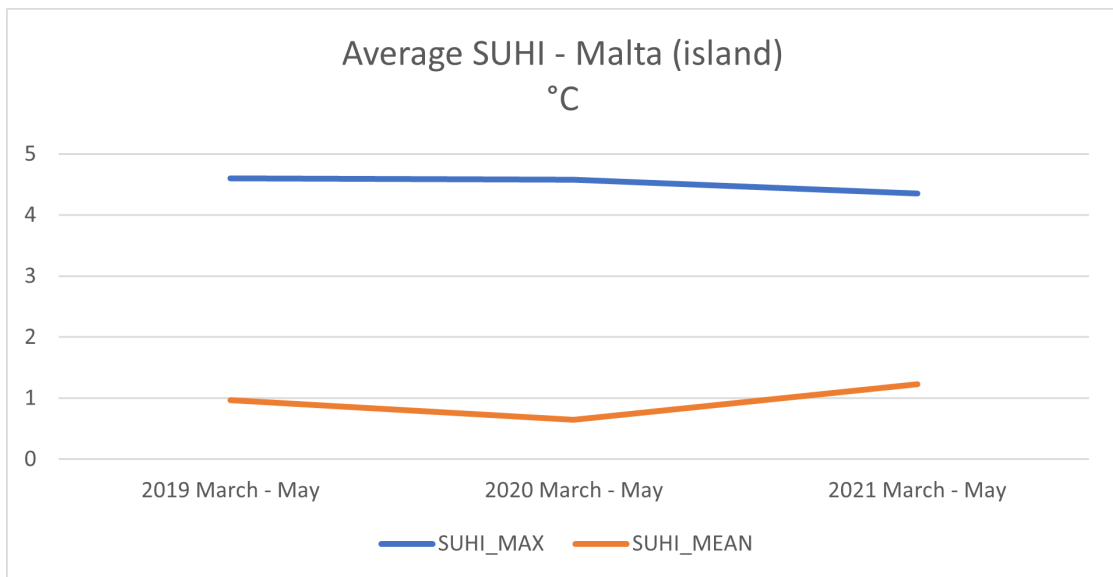


Figure 4.15: A line graph displaying the average  $SUHI_{MEAN}$  and  $SUHI_{MAX}$  across March, April and May for 2019 - 2021 for the Urban and Rural Areas of the Island of Malta.

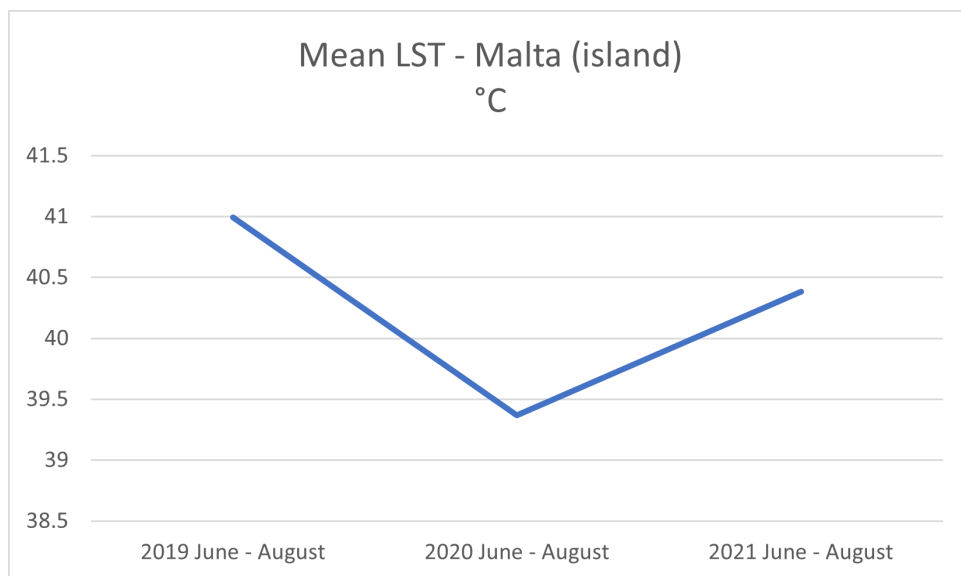


Figure 4.16: A line graph displaying the average Mean LST across June, July and August for 2019 - 2021 for the island of Malta.

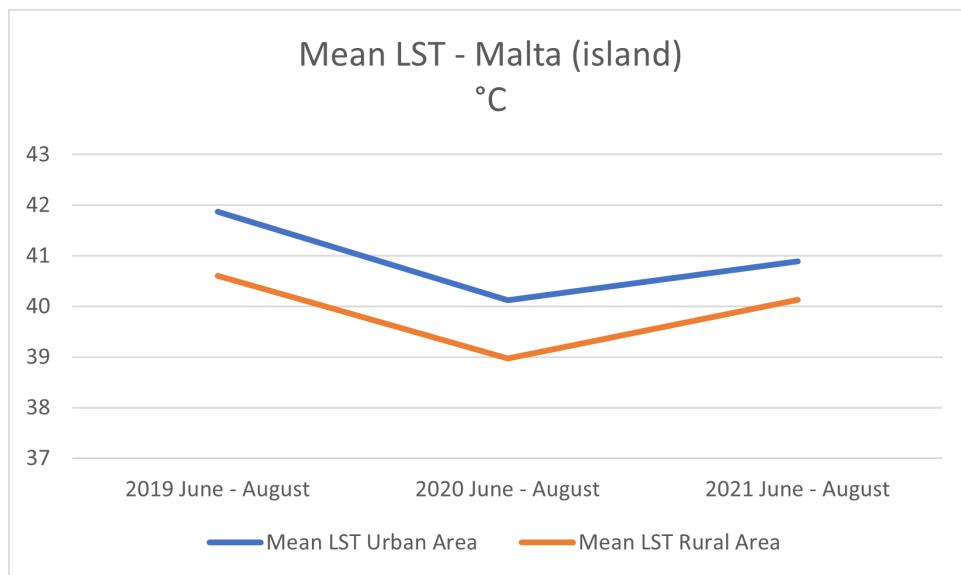


Figure 4.17: A line graph displaying the average Mean LST across June, July and August for 2019 - 2021 for the Urban and Rural Areas of the Island of Malta.

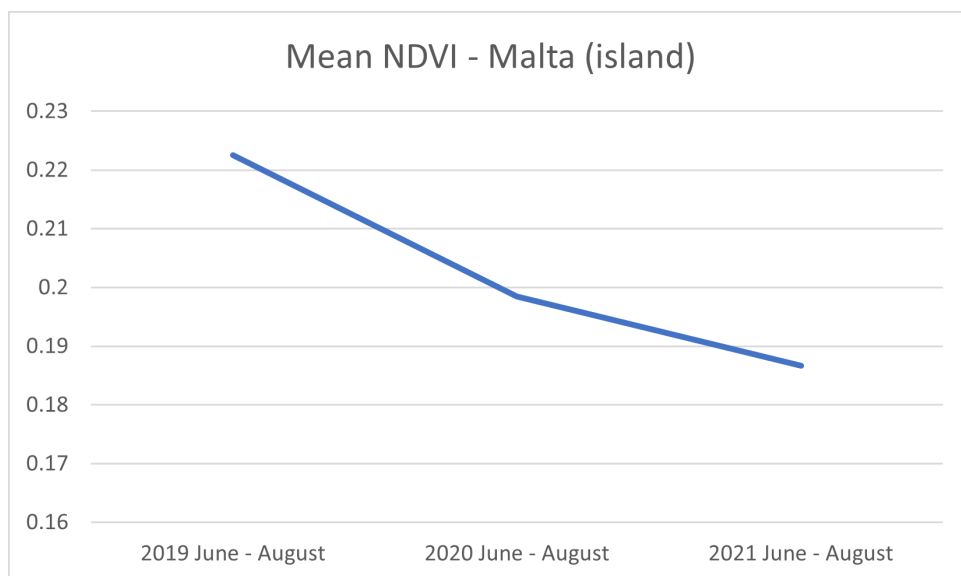


Figure 4.18: A line graph displaying the average Mean NDVI across June, July and August for 2019 - 2021 for the island of Malta.

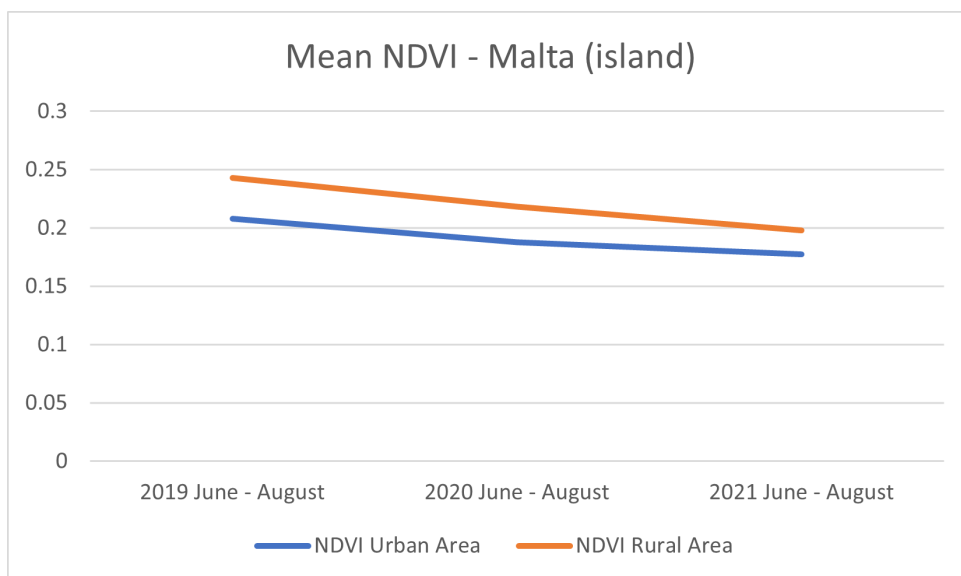


Figure 4.19: A line graph displaying the average Mean NDVI across June, July and August for 2019 - 2021 for the Urban and Rural Areas of the Island of Malta.

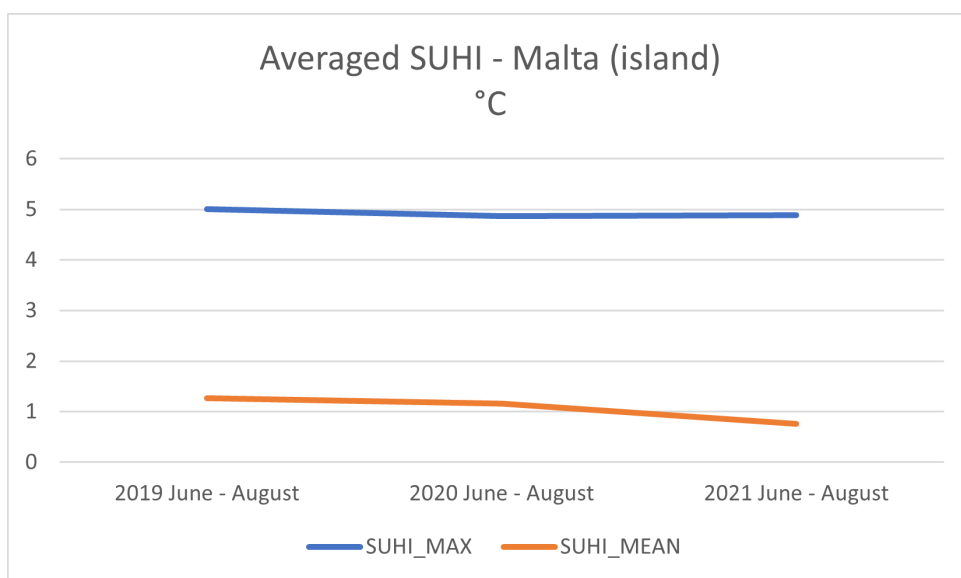


Figure 4.20: A line graph displaying the average  $SUHI_{MEAN}$  and  $SUHI_{MAX}$  across June, July and August for 2019 - 2021 for the Urban and Rural Areas of the Island of Malta.

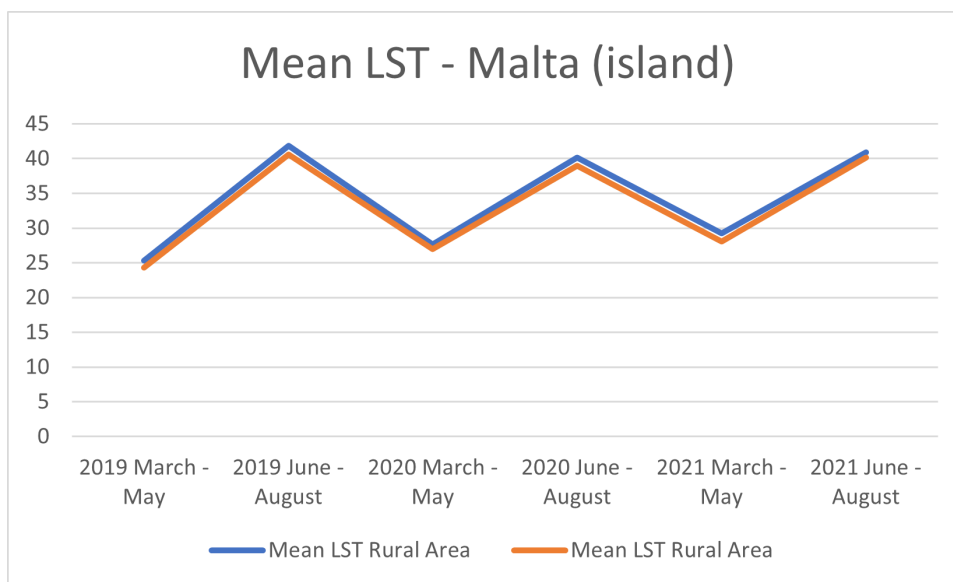


Figure 4.21: Mean LST processed in Line graph format across all periods

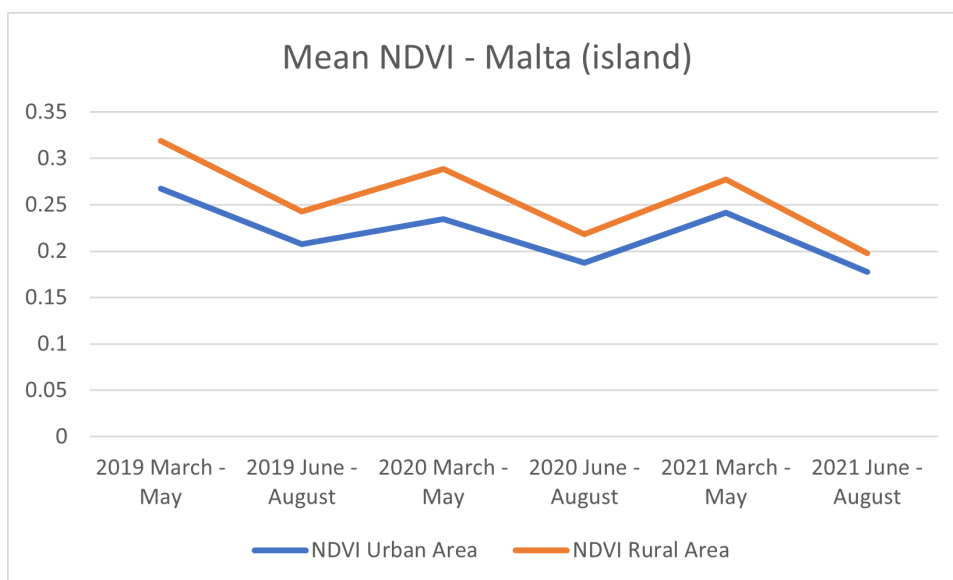


Figure 4.22: Mean NDVI processed in Line graph format across all periods

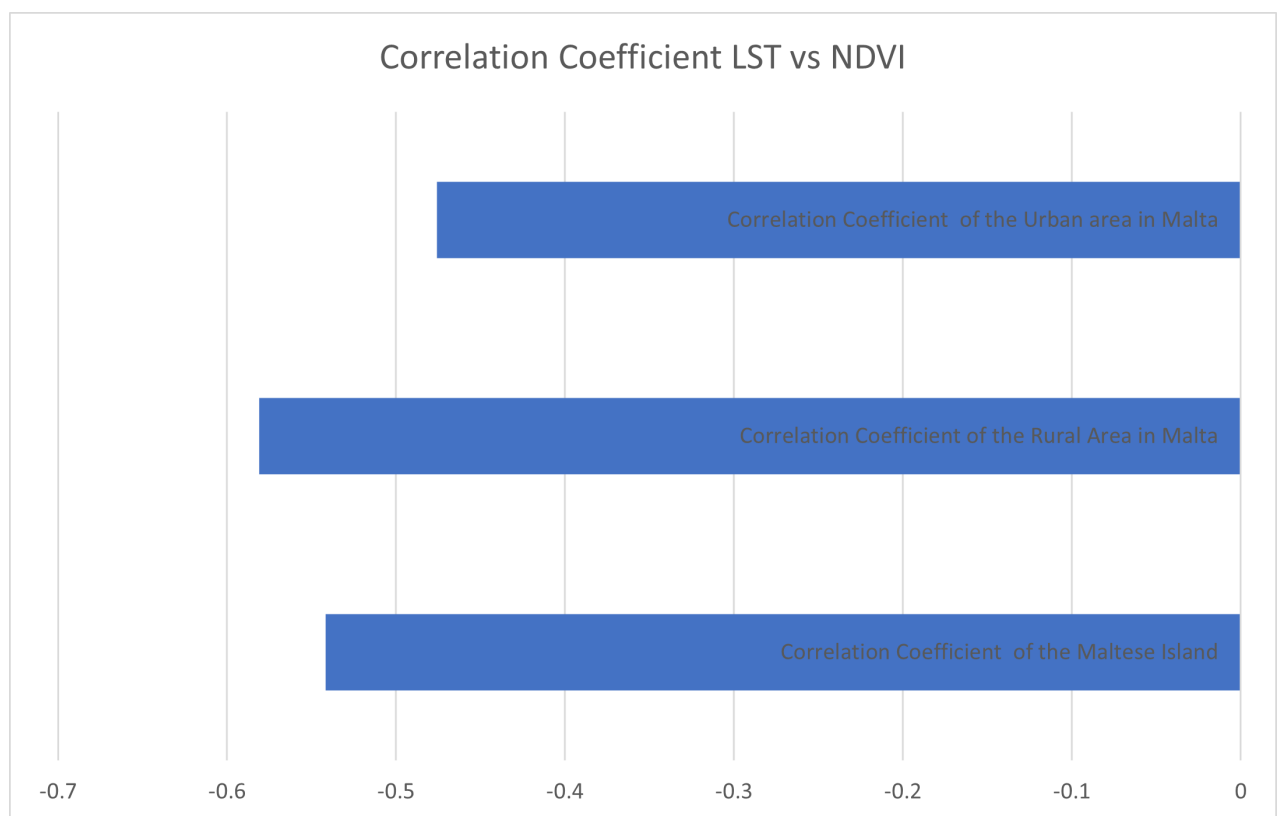


Figure 4.23: A bar graph displaying the correlation coefficient between Mean LST and Mean NDVI all periods studied

# Chapter 5

## Conclusion

### 5.1 Overview

The major goal of this study was to examine and observe UHI on the Maltese island using remote sensing technology. The Normalised Difference Vegetation Index (NDVI) has long been used to study temperature and vegetation; in fact, most of the research implies that NDVI and LST complement each other and have a relationship (Guo et al. 2012). As a result, in order to analyse and detect UHI, this study looked at vegetation levels and land surface temperatures, as done by García (2021). From March to August, from 2019 to 2021, 74 SLSTR Level-2 LST night-time products were obtained from the Sentinel-3 mission, freely available on the Copernicus database. These products served as a model for evaluating mean LST values over a period of time. Sentinel-3 has an NDVI band that was used in conjunction with the LST values recorded. Given the recent events of the pandemic and their societal implications, the months of March to May were used to watch UHI during pre-pandemic, during the pandemic, and after the pandemic. Meanwhile the months of June to August were utilised to better observe UHI and its rising presence on the Maltese Islands.

The free land cover products supplied by the European Space Agency Climate Change Initiative were used as a basis for the urban reference categorisation. By using the land cover data as reference, the Maltese archipelago was mapped using QGIS, an open-

source geographic information program that was used to assign geo-spatial vector data format. Due to the relative size of the islands, reference land cover data from ESA and Eurostat's description of Malta as being made up of two larger urban areas, "Valletta" and "Gozo", it was decided that the main island of Malta would be divided into two areas for this study, with the East side of Malta counting as the urban area and the West as the rural area.

Each product downloaded had to be re-projected to the Coordinate Reference System (CRS) EPSG:4326 using ESA's common architecture, Snap Desktop. This allowed the previously prepared shape files to create data frames from the areas of interest while also allowing the relevant pixel data to be found based on location. Cloud masking had to be applied to the products because the months of March and April are generally cloudy or wet.

Large amounts of satellite data were efficiently analysed utilising *snappy* by automating image processing activities with python scripts. The previous shape files developed for the research areas were then used to partition each product into different subsets, focusing on the Maltese main island, the urban area, and the rural area separately. By using Sobrino & Irakulis (2020)'s methodology and making use of the night-time obtained LST,  $SUHI_{MAX}$  and  $SUHI_{MEAN}$ , which can be described as thermal differences between the maximum and mean LST of the urban area and the LST surrounding area respectively, were used in order to better understand, track and observe the UHI effect.

For the observation part, UHI does indeed exist in Malta. It can also be seen how much thermal energy is retained in the Maltese landscape, with green spaces and vegetative areas emitting the least LST values and developed or barren areas emitting the most, confirming Stone et al. (2010)'s findings that UHI is caused by a decrease in vegetation, a higher prevalence of dark surfaces, and an increase in anthropogenic heat production. Peak LST could be seen in areas near urban areas, with areas such as the south of Malta, where the Maltese Freeport international port station and the Delimara Power Station are located, showing the extremes of human influence over a considerably larger area than what is typically expected. Considering the fact that Malta has double the sunshine hours

of other cities Northern Europe, these high LST values are to be expected, especially for the summer season when Malta averages 12 hours of continuous sunshine (July).

Overall, for the “Covid” period, an upward trend in LST values and a downward trend for NDVI was observed. Mean LST increased by 15% going from an averaged LST of 24.86°C in 2019 to 28.53°C in 2021. An interesting point about this period is that the increase in temperature was shared equally between the Rural and Urban areas. This means that the Rural area was not able to dissipate heat any quicker than the Urban area. A fascinating aspect of this time period is that the uptrend slowed slightly throughout the year 2020. This means that, while daily human activities aren’t enough to immediately reverse the upward trend, they are part of the larger picture when studying UHI. The “Summer” period, on the other hand, was the polar opposite of the “Covid” period. The Mean LST fell by 1.5% during this time period. Intriguingly, the mean LST decreased from 41°C in Summer 2019 to 39.4°C in Summer 2020. Then, in the summer of 2021, temperatures reach 40.4°C, nearly matching those of 2019.

The correlation between LST and NDVI was also investigated as part of this study. As previously discussed, LST and NDVI have been observed as having some type of correlation. By using all the products downloaded as a base and using the Mean LST and the Mean NDVI, a correlation pattern was confirmed. The main island of Malta was found of having a correlation coefficient of -0.54, the Rural Area has a correlation coefficient of -0.58, and the Urban Area has a correlation coefficient of -0.48. This disparity between the urban and rural areas raises the possibility that, while LST and NDVI are clearly correlated, other factors may be influencing NDVI’s effects on LST. The density of nearby water bodies or the water retention available in the air in the form of humidity or dew are the most obvious of these factors. Not to mention the inclusion of NDVI and topography of the study area, as mentioned in the previous chapter and in literature reviewed (Salvati et al. 2017, Martinelli et al. 2020, Kolokotsa et al. 2009).



## 5.2 Limitations and Recommendations

The idea of using a single remote sensing data source came with its disadvantages. The theory behind it was that by using a single data set, this research would avoid to go into exploring how varying ratings of inaccuracies between different satellites, would affect the final results. However, the inclusion of other satellites would be of greater importance as it would add more contextual data about the study area such as information on topography such as the Operational Land Imager (OLI) and Thermal Infrared Sensor (TIR) in LANDSAT 8 and the Enhanced Thematic Mapper (ETM+) in LANDSAT 7. With a greater arsenal of metrics, analysing and observing UHI would lead to a better understanding of the phenomena.

The use of land cover reference in this research could have been done in better detail. Instead of using the data as a visual reference and plotting manually the study areas, another recommendation would be to use the actual pixel values from the the land cover data and compare it with the relevant LST pixel value. A much more detailed perspective of this research would be possible with this method. On top of that, adding the inclusion of sun hours in correlation with LST or even vegetation height in coupled with NDVI could lead for more elaborate findings.

Whilst conducting this research it was noticed that apart from the obvious cloud coverage limitation that plague remote sensing satellites, Sentinel-3 had other issues. These issues came in the form of malfunctions and maintenance. Being an expensive probe, orbiting the Earth exposed to radiation, malfunctions are to be expected. Coupled with the fact that during winter, cloud coverage is almost constant, having a malfunction or maintenance schedule could be the difference between finding a product with cloud coverage or without. Therefore, during winter time, it is advisable to make use of local weather and data stations to track and monitor UHI in Malta. However, that does not make the summer period irrelevant, as this study proved by observing the extremities of the summer heat.

Processing multi-spectral images, although minimum requirements are not high, can draw an immense load on the processing machine. Full-orbital images hit the machine

worst, as a single processed image would amass around 30GB of data. Obviously to process that amount of data requires a great deal of processing power. As mentioned in this study methodology, a work around for this was to focus the reprojection process on the subset created in the initial phase of processing the data. Therefore investing in better equipment such as faster data storage, bigger memory and a more efficient processor would certainly make the analysis of greater time periods possible. An alternative would be exploring the possibilities that a Kubernetes system would achieve.

The location of the Sun in the sky may have influenced the final result's accuracy. This is due to the fact that the Earth's location on the Sun's orbital plane is always changing, therefore, the Sun's position in the sky fluctuates with the changing seasons (Tarng et al. 2018). This orbital shift impacts what is reflected back to the satellites' sensors, as well as the degree of shadowing on the ground, impacting the overall accuracy of the results (Ma et al. 2020).

# Appendix A

Covid			
Period	LST MEAN Malta	Mean LST Urban Area	Mean LST Rural Area
2019 March - May	24.85885838	25.32685198	24.35645403
2020 March - May	27.25360107	27.63571167	26.9939706
2021 March - May	28.52872408	29.26671659	28.03805072
Average	1.147628087	1.155560771	1.151154872

Figure A.1: March - May Averages for Mean LST

Covid			
Period	NDVI MEAN Malta	NDVI Urban Area	NDVI Rural Area
2019 March - May	0.289305533	0.267484494	0.318961784
2020 March - May	0.257575897	0.234384574	0.288680442
2021 March - May	0.256522065	0.241353402	0.277067841
Average	0.886682195	0.902308012	0.86865529

Figure A.2: March - May Averages for Mean NDVI

Covid		
Period	SUHI_MAX	SUHI_MEAN
2019 March - May	4.602262224	0.970397949
2020 March - May	4.577170236	0.641741071
2021 March - May	4.353177584	1.228665865
Average	0.945877782	1.266146395

Figure A.3: March - May Averages for  $SUHI_{MEAN}$  and  $SUHI_{MAX}$

Summer			
Period	LST_MEAN	Mean LST Urban Area	Mean LST Rural Area
2019 June - August	40.99493408	41.87300697	40.60096154
2020 June - August	39.36907255	40.12115713	38.96670767
2021 June - August	40.386	40.888	40.13469
Average	0.985146114	0.976476326	0.988515751

Figure A.4: June - August Averages for Mean LST

Summer			
Period	NDVI MEAN Malta	NDVI Urban Area	NDVI Rural Area
2019 June - August	0.222510769	0.207712964	0.242865046
2020 June - August	0.19845257	0.187669931	0.218227613
2021 June - August	0.18664	0.17729	0.197745
Average	0.838790863	0.853533629	0.814217621

Figure A.5: June - August Averages for Mean NDVI

Summer		
Period	SUHI_MAX	SUHI_MEAN
2019 June - August	5.002885085	1.272045429
2020 June - August	4.871295636	1.154449463
2021 June - August	4.880554	0.754036
Average	0.975547892	0.592774427

Figure A.6: June - August Averages for  $SUHI_{MEAN}$  and  $SUHI_{MAX}$

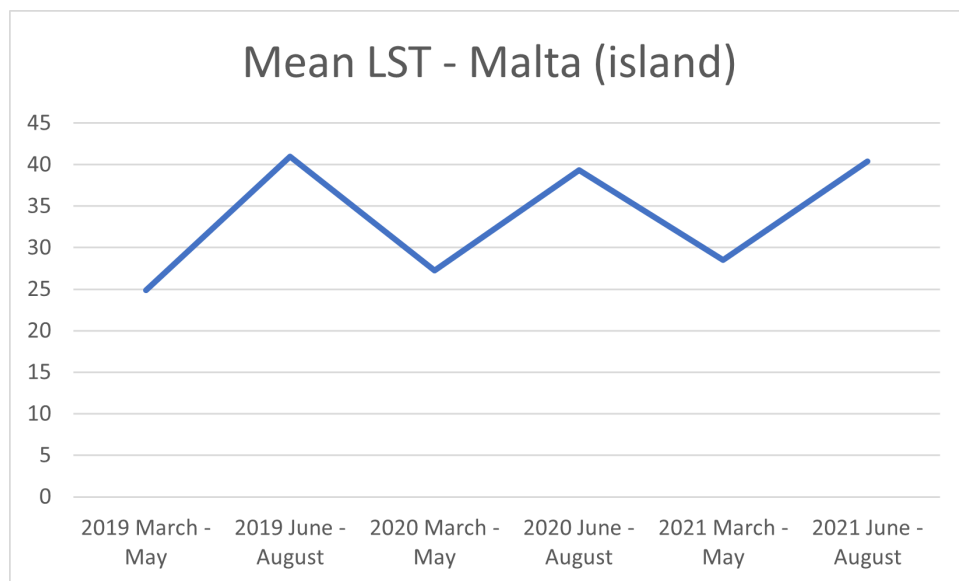


Figure A.7: Overall average Mean LST of Malta for all periods

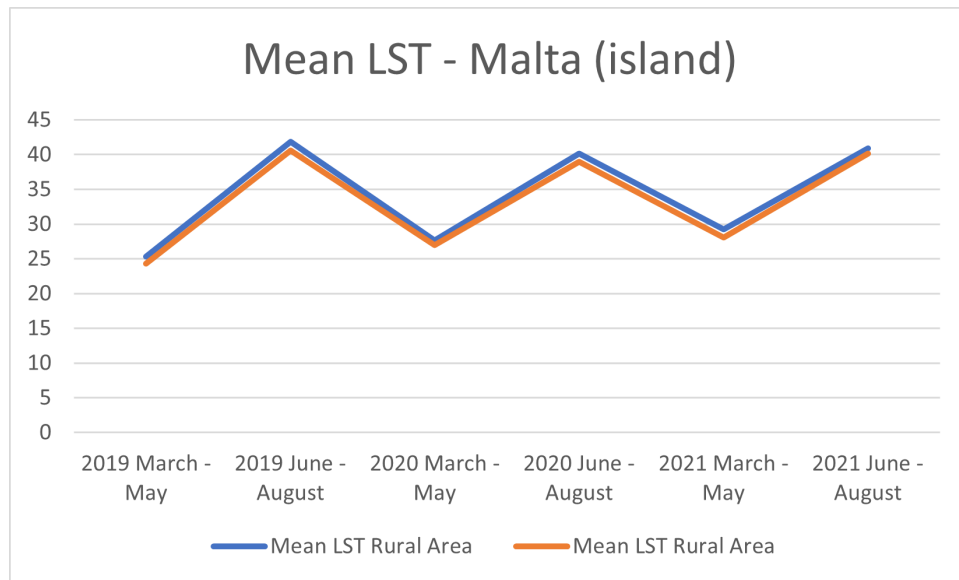


Figure A.8: Overall average Mean LST of the Urban and Rural areas for all periods

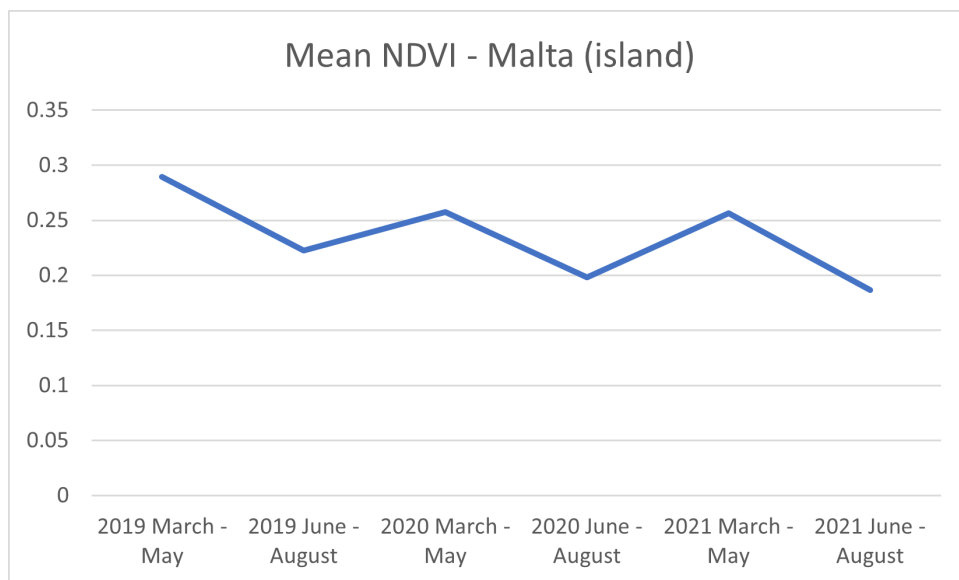


Figure A.9: Overall average Mean NDVI of Malta for all periods

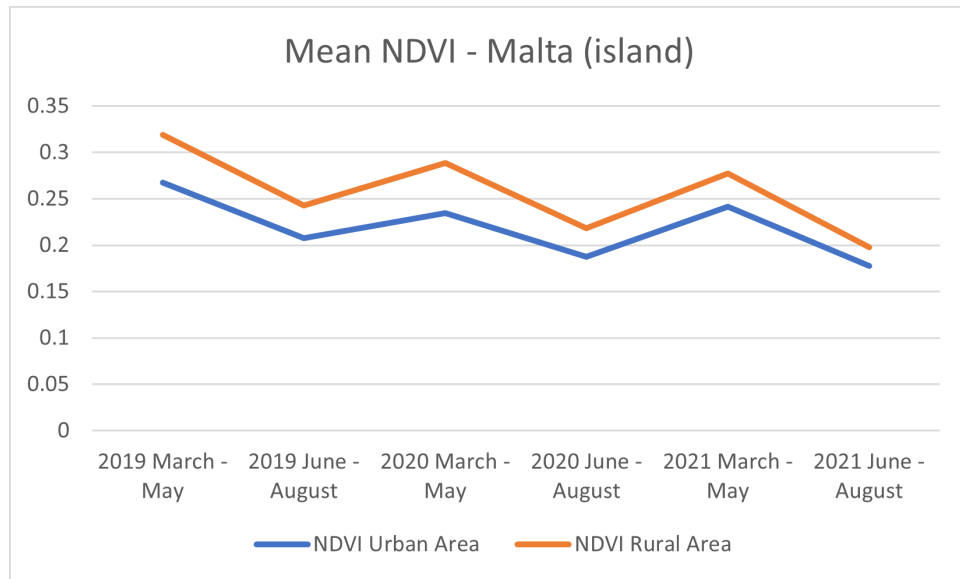


Figure A.10: Overall average Mean NDVI of the Urban and Rural areas for all periods

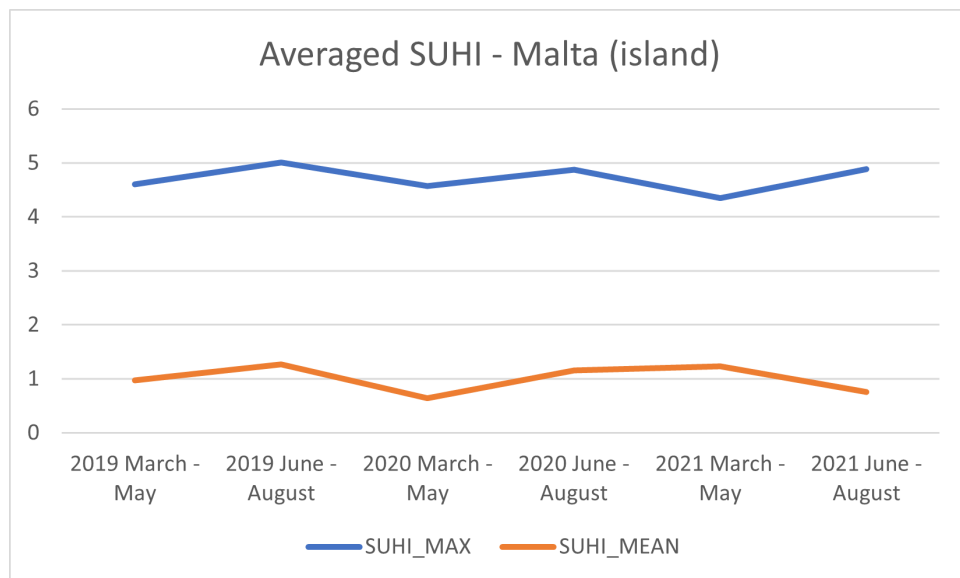


Figure A.11: Overall average  $SUHI_{MEAN}$  and  $SUHI_{MAX}$  of the Urban and Rural areas for all periods

Table A.1: Mean and Max LST for all products used for the study area of Malta(island)  
pt.1

	Date	Time	Satellite	LST_MEAN	LST_MAX
0	4/3/19	09:27	S3A	20.01403809	22.33599854
1	16/03/2019	09:16	S3A	16.02651978	20.51400757
2	17/03/2019	08:49	S3A	22.34832764	25.93200684
3	24/03/2019	09:08	S3A	22.92327881	26.77999878
4	20/04/2019	09:08	S3A	21.23800659	24.32199097
5	24/04/2019	09:05	S3A	22.04971313	24.89001465
6	27/04/2019	09:27	S3A	29.06033325	32.46798706
7	28/04/2019	09:01	S3A	28.13128662	32.93200684
8	1/5/19	09:23	S3A	28.70239258	32.56399536
9	2/5/19	08:57	S3A	25.33737183	30.75601196
10	5/5/19	09:20	S3A	25.66204834	29.60800171
11	10/5/19	08:50	S3A	27.05459595	32.79400635
12	17/05/2019	09:08	S3A	30.31134033	35.09399414
13	28/05/2019	09:23	S3A	29.1647644	34.84399414
14	4/6/19	09:42	S3A	36.37612915	40.48599243
15	5/6/19	09:16	S3A	39.10043335	43.25
16	9/6/19	09:12	S3A	44.64901733	50.22601318
17	16/06/2019	09:31	S3A	42.17428589	47.68200684
18	25/06/2019	08:57	S3A	37.87167358	41.60400391
19	2/7/19	09:16	S3A	42.80123901	48.79199219
20	13/07/2019	09:31	S3A	42.1194458	47.17800903
21	17/07/2019	09:27	S3A	41.33447266	45.79598999
22	26/07/2019	08:53	S3A	41.48660278	46.43399048
23	2/8/19	09:12	S3A	43.77093506	48.16000366
24	10/8/19	09:04	S3A	41.85916138	45.0880127
25	18/08/2019	08:57	S3A	39.54232788	43.98199463
26	22/08/2019	08:53	S3A	39.84841919	44.17199707
27	13/03/2020	08:51	S3A	23.91452026	26.60800171
28	20/03/2020	09:09	S3A	21.94940186	25.44799805
29	23/03/2020	09:32	S3A	17.54293823	23
30	24/03/2020	09:06	S3A	20.15997314	25.60400391
31	31/03/2020	09:24	S3A	21.15164185	24.29199219
32	4/4/20	08:41	S3B	16.05480957	20.6960144
33	9/4/20	08:51	S3A	24.22216797	29.84399414
34	13/04/2020	08:47	S3A	27.84884644	30.97799683
35	18/04/2020	09:19	S3B	29.83773804	34.5
36	28/04/2020	08:58	S3A	34.51870728	37.76998901
37	5/5/20	09:31	S3A	33.35269165	38.18399048

Table A.2: Mean and Max LST for all products used for the study area of Malta(island)  
pt.2

	Date	Time	Satellite	LST_MEAN	LST_MAX
38	12/5/20	09:10	S3B	37.83456421	42.65600586
39	16/05/2020	09:06	S3B	34.84771729	38.31399536
40	24/05/2020	09:38	S3A	38.31469727	44.57000732
41	4/6/20	09:14	S3B	35.85012817	39.04800415
42	14/06/2020	08:53	S3A	37.54644775	41.9119873
43	20/06/2020	09:38	S3A	39.70907593	43.67199707
44	28/06/2020	08:51	S3B	38.97570801	41.67800903
45	7/7/20	08:57	S3A	37.23931885	42.60400391
46	14/07/2020	09:16	S3A	39.76754761	44.61401367
47	21/07/2020	09:35	S3A	37.83929443	45.74398804
48	26/07/2020	09:05	S3A	42.71835327	46.97799683
49	3/8/20	08:57	S3A	39.79571533	44.45001221
50	13/08/2020	08:59	S3B	42.03631592	47.00201416
51	21/08/2020	08:51	S3B	40.78762817	44.86001587
52	28/08/2020	09:10	S3B	42.77279663	47.27999878
53	30/08/2020	08:57	S3A	36.75961304	40.18600464
54	6/3/21	09:23	S3A	18.47750854	21.96798706
55	12/3/21	09:29	S3B	20.0881958	23.96398926
56	25/03/2021	09:31	S3A	21.76220703	24.5880127
57	28/03/2021	09:14	S3B	25.72644043	28.9460144
58	31/03/2021	09:36	S3B	27.16879272	30.13198853
59	14/04/2021	09:12	S3A	28.53164673	31.88000488
60	25/04/2021	09:27	S3A	31.75723267	35.73199463
61	4/5/21	08:53	S3A	31.21734619	34.46398926
62	11/5/21	09:12	S3A	32.2935791	35.04800415
63	21/05/2021	09:14	S3B	33.75177002	39.56600952
64	25/05/2021	09:10	S3B	36.41998291	41.06399536
65	30/05/2021	09:20	S3A	39.82937622	47.01599121
66	4/6/21	08:50	S3A	34.72790527	38.11999512
67	11/6/21	09:08	S3A	41.61956787	46.30599976
68	4/7/21	09:12	S3A	43.86407471	47.4960022
69	19/07/2021	09:23	S3A	39.89752197	45.62600708
70	28/07/2021	08:50	S3A	40.81323242	45.63400269
71	7/8/21	08:52	S3B	41.18438721	44.08401489
72	14/08/2021	09:10	S3B	45.59307861	50.51998901
73	21/08/2021	09:29	S3B	35.38824463	42.76998901



Table A.3: Mean LST for all products used for The Urban and Rural Area pt.1

	Date	LST Mean Urban (East Malta)	LST Mean Rural (West Malta)
0	4/3/19	20.01794434	19.88018799
1	16/03/2019	16.00177002	16.13250732
2	17/03/2019	22.95755005	21.890625
3	24/03/2019	23.32913208	22.43804932
4	20/04/2019	21.35638428	20.97640991
5	24/04/2019	22.58209229	21.68273926
6	27/04/2019	29.52481079	28.81808472
7	28/04/2019	29.27819824	27.09747314
8	1/5/19	29.33062744	28.0713501
9	2/5/19	26.21640015	24.18389893
10	5/5/19	25.75891113	25.61419678
11	10/5/19	28.94671631	25.14129639
12	17/05/2019	31.14251709	29.5088501
13	28/05/2019	28.13287354	29.5546875
14	4/6/19	37.21047974	35.74539185
15	5/6/19	40.0027771	38.60928345
16	9/6/19	45.21438599	44.62548828
17	16/06/2019	43.11312866	41.90988159
18	25/06/2019	38.75491333	37.41860962
19	2/7/19	43.44522095	42.88153076
20	13/07/2019	43.09191895	41.23651123
21	17/07/2019	42.02072144	41.19137573
22	26/07/2019	42.13742065	41.2694397
23	2/8/19	44.77563477	43.24606323
24	10/8/19	42.58312988	41.57415771
25	18/08/2019	41.17391968	38.68579102
26	22/08/2019	40.82543945	39.41897583
27	13/03/2020	24.58270264	23.26116943
28	20/03/2020	22.17114258	21.49053955
29	23/03/2020	17.93438721	17.82019043
30	24/03/2020	19.05935669	20.79754639
31	31/03/2020	21.56741333	20.61575317
32	4/4/20	15.27474976	17.16558838
33	9/4/20	24.84622192	23.40823364
34	13/04/2020	28.45211792	27.29650879
35	18/04/2020	30.01766968	29.72323608
36	28/04/2020	35.31774902	34.02651978
37	5/5/20	34.22714233	32.77297974

Table A.4: Mean LST for all products used for The Urban and Rural Area pt.2

	Date	LST Mean Urban (East Malta)	LST Mean Rural (West Malta)
38	12/5/20	38.73947144	37.24206543
39	16/05/2020	35.2512207	34.87948608
40	24/05/2020	39.45861816	37.41577148
41	4/6/20	36.13983154	35.41760254
42	14/06/2020	38.10351563	37.24661255
43	20/06/2020	40.35043335	39.30184937
44	28/06/2020	39.74057007	38.61566162
45	7/7/20	39.12576294	35.90026855
46	14/07/2020	40.13723755	40.12814331
47	21/07/2020	38.58633423	37.3404541
48	26/07/2020	43.72210693	41.98114014
49	3/8/20	40.77926636	39.29556274
50	13/08/2020	42.95227051	41.73617554
51	21/08/2020	41.66226196	40.3553772
52	28/08/2020	43.50793457	42.415802
53	30/08/2020	36.76751709	36.83255005
54	6/3/21	18.28414917	18.33810425
55	12/3/21	20.16162109	19.45993042
56	25/03/2021	21.9642334	21.69723511
57	28/03/2021	25.68200684	25.81988525
58	31/03/2021	27.38659668	27.08233643
59	14/04/2021	28.73434448	28.4543457
60	25/04/2021	32.39172363	31.3125
61	4/5/21	31.92077637	31.06243896
62	11/5/21	32.59313965	32.14712524
63	21/05/2021	34.86520386	32.06442261
64	25/05/2021	37.18023682	36.23876953
65	30/05/2021	40.83126831	39.27957153
66	4/6/21	35.61795044	34.44064331
67	11/6/21	42.48059082	41.28411865
68	4/7/21	44.55859375	43.56610107
69	19/07/2021	40.61080933	39.14520264
70	28/07/2021	41.42059326	40.6305542
71	7/8/21	41.88546753	40.88775635
72	14/08/2021	46.42776489	45.33828735
73	21/08/2021	34.10809326	35.78491211

Table A.5: Max LST for all products used for The Urban and Rural Area pt.1

	Date	LST Max Urban (East Malta)	LST Max Rural (West Malta)
0	4/3/19	22.33599854	21.20001221
1	16/03/2019	20.51400757	20.51400757
2	17/03/2019	25.93200684	25.93200684
3	24/03/2019	26.77999878	24.89001465
4	20/04/2019	24.32199097	23.93600464
5	24/04/2019	24.89001465	24.04000854
6	27/04/2019	32.46798706	32.46798706
7	28/04/2019	32.93200684	31.38598633
8	1/5/19	32.56399536	31.14801025
9	2/5/19	30.75601196	28.54400635
10	5/5/19	29.60800171	29.57199097
11	10/5/19	32.79400635	32.07800293
12	17/05/2019	35.09399414	33.6000061
13	28/05/2019	34.43200684	34.84399414
14	4/6/19	40.48599243	39.61999512
15	5/6/19	43.25	43.25
16	9/6/19	50.22601318	50.22601318
17	16/06/2019	47.68200684	47.68200684
18	25/06/2019	41.60400391	41.20800781
19	2/7/19	48.79199219	48.79199219
20	13/07/2019	47.17800903	45.85198975
21	17/07/2019	45.79598999	45.79598999
22	26/07/2019	46.43399048	46.43399048
23	2/8/19	48.16000366	48.11401367
24	10/8/19	45.0880127	45.0880127
25	18/08/2019	43.98199463	43.98199463
26	22/08/2019	44.17199707	44.17199707
27	13/03/2020	26.60800171	25.63000488
28	20/03/2020	25.44799805	25.44799805
29	23/03/2020	23	23
30	24/03/2020	25.31399536	25.60400391
31	31/03/2020	24.29199219	22.48400879
32	4/4/20	20.53201294	20.6960144
33	9/4/20	29.84399414	29.84399414
34	13/04/2020	30.97799683	30.62600708
35	18/04/2020	34.5	33.01998901
36	28/04/2020	37.76998901	37.61199951
37	5/5/20	38.18399048	38.18399048

Table A.6: Max LST for all products used for The Urban and Rural Area pt.2

	Date	LST Max Urban (East Malta)	LST Max Rural (West Malta)
38	12/5/20	42.65600586	41.06399536
39	16/05/2020	38.29998779	38.31399536
40	24/05/2020	44.57000732	42.23400879
41	4/6/20	39.04800415	38.83200073
42	14/06/2020	41.9119873	41.9119873
43	20/06/2020	43.67199707	43.30599976
44	28/06/2020	41.67800903	41.67800903
45	7/7/20	42.60400391	40.45999146
46	14/07/2020	44.48001099	44.61401367
47	21/07/2020	45.74398804	44.14801025
48	26/07/2020	46.97799683	46.97799683
49	3/8/20	44.45001221	42.97601318
50	13/08/2020	47.00201416	47.00201416
51	21/08/2020	44.86001587	43.53799438
52	28/08/2020	47.27999878	46.88000488
53	30/08/2020	40.18600464	40.18600464
54	6/3/21	21.96798706	21.7460022
55	12/3/21	23.96398926	23.21798706
56	25/03/2021	24.1499939	24.5880127
57	28/03/2021	27.73199463	28.9460144
58	31/03/2021	30.02999878	30.13198853
59	14/04/2021	31.88000488	31.35598755
60	25/04/2021	35.73199463	35.73199463
61	4/5/21	34.46398926	34.46398926
62	11/5/21	35.04800415	34.49398804
63	21/05/2021	39.56600952	37.52200317
64	25/05/2021	41.06399536	41.06399536
65	30/05/2021	47.01599121	45.04199219
66	4/6/21	38.11999512	38.11999512
67	11/6/21	46.30599976	46.30599976
68	4/7/21	47.4960022	47.4960022
69	19/07/2021	45.62600708	43.78201294
70	28/07/2021	45.63400269	45.63400269
71	7/8/21	44.08401489	44.01199341
72	14/08/2021	50.51998901	50.11801147
73	21/08/2021	42.33599854	42.76998901

Table A.7: Mean NDVI for all products used for Malta, the Urban and Rural Area pt.1

	Date	Mean NDVI Malta	Mean NDVI Urban	Mean NDVI Rural
0	4/3/19	0.43252257	0.41041943	0.467879
1	16/03/2019	0.18279155	0.15702169	0.21868396
2	17/03/2019	0.37107667	0.3594616	0.40088332
3	24/03/2019	0.39777386	0.37107325	0.44340742
4	20/04/2019	0.27849576	0.25547358	0.30128124
5	24/04/2019	0.23941274	0.22359602	0.25937977
6	27/04/2019	0.3185815	0.29122305	0.35212186
7	28/04/2019	0.29888228	0.28302595	0.32405478
8	1/5/19	0.3273064	0.29291457	0.36602136
9	2/5/19	0.27030563	0.24655786	0.2976496
10	5/5/19	0.25206733	0.22746448	0.28808483
11	10/5/19	0.23243938	0.24202745	0.23242304
12	17/05/2019	0.25396472	0.23433934	0.27999842
13	28/05/2019	0.19465707	0.15018465	0.23359638
14	4/6/19	0.24481647	0.21930073	0.27786216
15	5/6/19	0.24582781	0.22505233	0.2701422
16	9/6/19	0.22529548	0.20504725	0.24541865
17	16/06/2019	0.22475173	0.20611477	0.24673498
18	25/06/2019	0.21561487	0.20292693	0.234975
19	2/7/19	0.2251702	0.20422016	0.25275326
20	13/07/2019	0.22753341	0.20706667	0.25066003
21	17/07/2019	0.22469024	0.20975591	0.24664924
22	26/07/2019	0.22536403	0.21181665	0.2443683
23	2/8/19	0.21126314	0.2005407	0.22823265
24	10/8/19	0.20915388	0.1995609	0.2241008
25	18/08/2019	0.20251727	0.20339072	0.21229717
26	22/08/2019	0.21064147	0.20547481	0.22305116
27	13/03/2020	0.3571816	0.32463	0.39969647
28	20/03/2020	0.29743904	0.26740658	0.32658583
29	23/03/2020	0.13309097	0.12417507	0.15745607
30	24/03/2020	0.19642137	0.15169013	0.2360717
31	31/03/2020	0.33812803	0.30979055	0.37633055
32	4/4/20	0.22900596	0.20620257	0.27843177
33	9/4/20	0.26467112	0.25022545	0.28333977
34	13/04/2020	0.31593	0.29813844	0.343901
35	18/04/2020	0.29721016	0.2698189	0.33737835
36	28/04/2020	0.2779616	0.25342458	0.31006783
37	5/5/20	0.23081122	0.21275188	0.25764483

Table A.8: Mean NDVI for all products used for Malta, the Urban and Rural Area pt.2

	Date	Mean NDVI Malta	Mean NDVI Urban	Mean NDVI Rural
38	12/5/20	0.2352845	0.22044295	0.25766528
39	16/05/2020	0.20611323	0.1892472	0.22768594
40	24/05/2020	0.22681376	0.20343974	0.2492708
41	4/6/20	0.21847118	0.20189504	0.23943345
42	14/06/2020	0.2125187	0.2013624	0.23132984
43	20/06/2020	0.21092802	0.19494039	0.23908211
44	28/06/2020	0.211001	0.20049885	0.2334455
45	7/7/20	0.19931886	0.19604805	0.21445711
46	14/07/2020	0.18512307	0.16539192	0.2155434
47	21/07/2020	0.1816605	0.15595116	0.21220303
48	26/07/2020	0.21087945	0.20246287	0.22806364
49	3/8/20	0.18996102	0.18204628	0.21117826
50	13/08/2020	0.1972988	0.19540334	0.20914589
51	21/08/2020	0.19680455	0.19096519	0.21058154
52	28/08/2020	0.190751	0.18538284	0.20567656
53	30/08/2020	0.17516726	0.16736077	0.18681864
54	6/3/21	0.24600025	0.21608992	0.27506968
55	12/3/21	0.31599507	0.29356715	0.3336097
56	25/03/2021	0.3422435	0.3257393	0.37036783
57	28/03/2021	0.3224139	0.29772	0.3605965
58	31/03/2021	0.33645883	0.3231079	0.36093816
59	14/04/2021	0.27962402	0.26045075	0.30614132
60	25/04/2021	0.23739128	0.23103243	0.2453723
61	4/5/21	0.22231403	0.21454114	0.2381645
62	11/5/21	0.20818105	0.18949507	0.22851773
63	21/05/2021	0.1835518	0.1797103	0.18739708
64	25/05/2021	0.1889513	0.17612538	0.20650846
65	30/05/2021	0.21224771	0.19565718	0.23301189
66	4/6/21	0.2138545	0.20596811	0.22640435
67	11/6/21	0.21645151	0.20602463	0.2316164
68	4/7/21	0.19109087	0.18103927	0.20304096
69	19/07/2021	0.18860136	0.17510912	0.20159267
70	28/07/2021	0.17972422	0.1805492	0.18504316
71	7/8/21	0.18701172	0.17901705	0.1969889
72	14/08/2021	0.1843082	0.1788552	0.19337007
73	21/08/2021	0.13215555	0.11180749	0.14390191

Table A.9: SUHI\_MAX and SUHI\_MEAN for all products used for The Urban and Rural Area pt.1

	Date	SUHI_MAX	SUHI_MEAN
0	4/3/19	2.455810547	0.137756348
1	16/03/2019	4.381500244	-0.130737305
2	17/03/2019	4.041381836	1.066925049
3	24/03/2019	4.341949463	0.891082764
4	20/04/2019	3.345581055	0.379974365
5	24/04/2019	3.207275391	0.899353027
6	27/04/2019	3.649902344	0.706726074
7	28/04/2019	5.834533691	2.180725098
8	1/5/19	4.492645264	1.259277344
9	2/5/19	6.572113037	2.032501221
10	5/5/19	3.993804932	0.144714355
11	10/5/19	7.652709961	3.805419922
12	17/05/2019	5.585144043	1.633666992
13	28/05/2019	4.877319336	-1.421813965
14	4/6/19	4.740600586	1.465087891
15	5/6/19	4.640716553	1.393493652
16	9/6/19	5.600524902	0.588897705
17	16/06/2019	5.772125244	1.20324707
18	25/06/2019	4.185394287	1.336303711
19	2/7/19	5.910461426	0.563690186
20	13/07/2019	5.941497803	1.855407715
21	17/07/2019	4.604614258	0.829345703
22	26/07/2019	5.164550781	0.867980957
23	2/8/19	4.91394043	1.529571533
24	10/8/19	3.51385498	1.008972168
25	18/08/2019	5.296203613	2.488128662
26	22/08/2019	4.75302124	1.406463623
27	13/03/2020	3.346832275	1.321533203
28	20/03/2020	3.957458496	0.680603027
29	23/03/2020	5.17980957	0.114196777
30	24/03/2020	4.516448975	-1.738189697
31	31/03/2020	3.676239014	0.951660156
32	4/4/20	3.366424561	-1.890838623
33	9/4/20	6.435760498	1.437988281
34	13/04/2020	3.681488037	1.155609131
35	18/04/2020	4.776763916	0.294433594
36	28/04/2020	3.743469238	1.291229248
37	5/5/20	5.411010742	1.454162598

Table A.10: SUHI\_MAX and SUHI\_MEAN for all products used for The Urban and Rural Area pt.2

	Date	SUHI_MAX	SUHI_MEAN
38	12/5/20	5.41394043	1.497406006
39	16/05/2020	3.420501709	0.371734619
40	24/05/2020	7.15423584	2.04284668
41	4/6/20	3.630401611	0.722229004
42	14/06/2020	4.665374756	0.856903076
43	20/06/2020	4.370147705	1.048583984
44	28/06/2020	3.062347412	1.124908447
45	7/7/20	6.703735352	3.225494385
46	14/07/2020	4.351867676	0.009094238
47	21/07/2020	8.403533936	1.245880127
48	26/07/2020	4.996856689	1.740966797
49	3/8/20	5.154449463	1.483703613
50	13/08/2020	5.265838623	1.216094971
51	21/08/2020	4.504638672	1.306884766
52	28/08/2020	4.864196777	1.092132568
53	30/08/2020	3.35345459	-0.065032959
54	6/3/21	3.629882813	-0.053955078
55	12/3/21	4.504058838	0.701690674
56	25/03/2021	2.452758789	0.266998291
57	28/03/2021	1.912109375	-0.137878418
58	31/03/2021	2.947662354	0.304260254
59	14/04/2021	3.42565918	0.279998779
60	25/04/2021	4.419494629	1.079223633
61	4/5/21	3.401550293	0.858337402
62	11/5/21	2.900878906	0.446014404
63	21/05/2021	7.501586914	2.80078125
64	25/05/2021	4.82522583	0.941467285
65	30/05/2021	7.736419678	1.551696777
66	4/6/21	3.679351807	1.177307129
67	11/6/21	5.021881104	1.196472168
68	4/7/21	3.929901123	0.992492676
69	19/07/2021	6.480804443	1.465606689
70	28/07/2021	5.003448486	0.790039063
71	7/8/21	3.196258545	0.997711182
72	14/08/2021	5.18170166	1.089477539
73	21/08/2021	6.551086426	-1.676818848



Table A.11: Weather Station Report of each product date pt.1

Date	Temperature (°C) AVG	Humidity (%) AVG	Wind Speed (km/h) AVG
4/3/19	13.4	78.7	7.3
16/03/2019	14.1	82.1	16.3
17/03/2019	15	77.8	15.2
24/03/2019	14.8	77.1	9.5
20/04/2019	15.6	80.3	27.7
24/04/2019	17.1	88.3	19.9
27/04/2019	18.1	76.2	17.1
28/04/2019	16.8	71.1	17.9
1/5/19	16	70.7	12.9
2/5/19	16	72.3	9.8
5/5/19	16.7	70.2	30.5
10/5/19	16.5	63.5	8
17/05/2019	16.4	75.6	14.6
28/05/2019	20.3	65.3	18.3
4/6/19	22.1	60.6	19
5/6/19	22.3	62.5	16.4
9/6/19	29.4	29.3	9.5
16/06/2019	28.3	47.7	8.9
25/06/2019	27	68.4	11.8
2/7/19	26.5	62	9.2
13/07/2019	27.5	66.1	21.2
17/07/2019	25.5	58.4	13.3
26/07/2019	27.9	63.9	8.9
2/8/19	28.6	54.1	11.1
10/8/19	28.4	77.3	15.5
18/08/2019	26.7	69	10.3
22/08/2019	27.1	67.6	9
13/03/2020	15.9	78.1	17.9
20/03/2020	14.3	70.7	24.4
23/03/2020	14.4	87.6	12.7
24/03/2020	14	84.9	22.3
31/03/2020	14	79.6	13.2
4/4/20	13.6	84.7	22.4
9/4/20	14.5	78.9	11.8
13/04/2020	15	81.6	16.1
18/04/2020	17.2	84.7	7.2
28/04/2020	19.7	71.2	9.8
5/5/20	19	85.5	12.3

Table A.12: Weather Station Report of each product date pt.2

Date	Temperature (°C) AVG	Humidity (%) AVG	Wind Speed (km/h) AVG
12/5/20	22.6	52.6	13.2
16/05/2020	24.3	63.6	21.9
24/05/2020	21.5	56.3	11.7
4/6/20	21.4	79.1	22
14/06/2020	24.9	54.9	11.5
20/06/2020	25	3.2	27.2
28/06/2020	24.8	72.8	9.8
7/7/20	24.8	73.8	22.8
14/07/2020	26	77	8.2
21/07/2020	25.1	74.7	7.9
26/07/2020	27.5	70.4	12.5
3/8/20	29	72	9.3
13/08/2020	28.5	57.7	9.4
21/08/2020	27.9	68.7	5.9
28/08/2020	27.6	71.6	7.8
30/08/2020	27.7	82.9	17.3
6/3/21	14.6	88.9	13.9
12/3/21	12.6	73.1	13.3
25/03/2021	12.4	65.8	15.1
28/03/2021	15.4	87	13.4
31/03/2021	15	70.1	9.8
14/04/2021	14.5	65.3	15.1
25/04/2021	16.2	75.8	14.8
4/5/21	18.8	69.2	13.6
11/5/21	19.6	78.5	20.2
13/05/2021	18.4	68.6	19.3
21/05/2021	19.5	65.1	14.1
25/05/2021	21.8	70.2	10.2
30/05/2021	22.4	60.2	12.3
4/6/21	22.1	68.6	11.2
11/6/21	23.2	65.8	9.1
4/7/21	28.8	59.5	10.9
19/07/2021	25.4	71.4	17.1
28/07/2021	29.7	38.6	10.1
7/8/21	28.8	64	16.6
14/08/2021	29.5	67.5	8.5
21/08/2021	27.1	73.6	8.3

# Bibliography

- Akbari, H. & Rose, L. S. (2008), 'Urban surfaces and heat island mitigation potentials', *Journal of the Human-Environment System* **11**(2), 85–101.
- Arnfield, A. J. (2003), 'Two decades of urban climate research: a review of turbulence, exchanges of energy and water, and the urban heat island.', *International journal of climatology* **23**, 1–26.
- Barbieri, T., Despini, F. & Teggi, S. (2018), 'A multi-temporal analyses of land surface temperature using landsat-8 data and open source software: The case study of modena, italy', *Sustainability* **10**(5), 1678.
- Bhatta, B., Saraswati, S. & Bandyopadhyay, D. (2010), 'Urban sprawl measurement from remote sensing data', *Applied Geography* **30**(4), 731–740. Climate Change and Applied Geography – Place, Policy, and Practice.  
**URL:** <https://www.sciencedirect.com/science/article/pii/S0143622810000226>
- Bian, F., Fan, D., Zhang, Y. & Wang, D. (2018), 'Synchronous atmospheric radiation correction of gf - 2 satellite multispectral image.', p. 10697.
- CaiyanWu, Li, J., Wang, C., Song, C., Chen, Y., Finka, M. & Rosa, D. L. (2019), 'Understanding the relationship between urban blue infrastructure and land surface temperature', *Science of The Total Environment* **694**.
- Cardelino, C. & Chameides, W. (1990), 'Natural hydrocarbons, urbanization, and urban ozone', *Journal of Geophysical Research* **95**, 13,971–13,979.

- Carlson, T. N., Dodd, J. K., Benjamin, S. G. & Cooper, J. N. (1981), 'Satellite estimation of the surface energy balance, moisture availability and thermal inertia', *Journal of Applied Meteorology* **20**, 67–87.
- Caselles, V. & Lopez Garcia, M. (1989), 'An alternative simple approach to estimate atmospheric correction in multitemporal studies', *International Journal of Remote Sensing* **10**(6), 1127–1134.
- Cheng, J., Liang, S., Wang, J. & Li, X. (2009), 'A stepwise refining algorithm of temperature and emissivity separation for hyperspectral thermal infrared data', *IEEE Transactions on Geoscience and Remote Sensing* **48**(3), 1588–1597.
- Elachi, C. & Van Zyl, J. J. (2021), *Introduction to the physics and techniques of remote sensing*, John Wiley & Sons.
- Galster, G., Hanson, R., Ratcliffe, M., Wolman, H., Coleman, S. & Freihage, J. (2001), 'Wrestling sprawl to the ground: Defining and measuring an elusive concept', *Housing Policy Debate* **12**, 681–717.
- García, D. H. (2021), 'Analysis of urban heat island and heat waves using sentinel-3 images: a study of andalusian cities in spain.', *Earth Syst Environ* .
- Ghent, D., Veal, K., Trent, T., Dodd, E., Sembhi, H. & Remedios, J. (2019), 'A new approach to defining uncertainties for modis land surface temperature', *Remote Sensing* **11**(9), 1021.
- Guo, Z., Wang, S., Cheng, M. & Shu, Y. (2012), 'Assess the effect of different degrees of urbanization on land surface temperature using remote sensing images', *Procedia Environmental Sciences* **13**, 935–942.
- Hadjimitsis, D. G., Papadavid, G., Agapiou, A., Themistocleous, K., Hadjimitsis, M., Retalis, A., Michaelides, S., Chrysoulakis, N., Toullos, L. & Clayton, C. (2010), 'Atmospheric correction for satellite remotely sensed data intended for agricultural appli-

- cations: impact on vegetation indices’, *Natural Hazards and Earth System Sciences* **10**(1), 89–95.
- Hidalgo García, D. (2021), ‘Analysis and precision of the terrestrial surface temperature using landsat 8 and sentinel 3 images: Study applied to the city of granada (spain)’, *Sustainable Cities and Society* **71**, 102980.  
**URL:** <https://www.sciencedirect.com/science/article/pii/S2210670721002663>
- Hidalgo García, D. & Arco Díaz, J. (2021), ‘Modeling of the urban heat island on local climatic zones of a city using sentinel 3 images: Urban determining factors’, *Urban Climate* **37**, 100840.  
**URL:** <https://www.sciencedirect.com/science/article/pii/S2212095521000705>
- Hu, Y., Dai, Z. & Guldmann, J.-M. (2020), ‘Modeling the impact of 2d/3d urban indicators on the urban heat island over different seasons: A boosted regression tree approach’, *Journal of Environmental Management* **266**, 110424.
- Ilori, C. O., Pahlevan, N. & Knudby, A. (2019), ‘Analyzing performances of different atmospheric correction techniques for landsat 8: application for coastal remote sensing’, *Remote Sensing* **11**(4), 469.
- Jensen, J. (1996), ‘Introductory digital image processing: A remote sensing perspective’, *Prentice Hall, Inc.* pp. 197–256.
- Jensen, J. R. (1986), *Introductory digital image processing: a remote sensing perspective*, Technical report, Univ. of South Carolina, Columbus.
- Jiang, S., Lee, X., Wang, J. & Wang, K. (2019), ‘Amplified urban heat islands during heat wave periods’, *Journal of Geophysical Research: Atmospheres* **124**(14), 7797–7812.
- Karakuş, C. B. (2019), ‘The impact of land use/land cover (lulc) changes on land surface temperature in sivas city center and its surroundings and assessment of urban heat island’, *Asia-Pacific Journal of Atmospheric Sciences volume* **55**, 669–684.

- Karl, T. R., Diaz, H. F. & Kukla, G. (1988), 'Urbanization: Its detection and effect in the united states climate record.', *Journal of Climate* **1**, 1099–1123.
- Keeratikasikorn, C. & Bonafoni, S. (2018), 'Urban heat island analysis over the land use zoning plan of bangkok by means of landsat 8 imagery', *Remote Sensing* **10**(3), 440.
- Khalaf, A. (2018), Utilization of thermal bands of landsat 8 data and geographic information system for analysis of urban heat island in baghdad governorate 2016, in 'MATEC Web of Conferences', Vol. 162, EDP Sciences, p. 03026.
- Kolokotsa, D., Psomas, A. & Karapidakis, E. (2009), 'Urban heat island in southern europe: The case study of hania, crete', *Solar Energy* **83**(10), 1871–1883.
- Landsberg, H. (1981), in 'The Urban Climate', Academic Press, New York, NY, USA.
- Lemus-Canovas, M., Martin-Vide, J., Moreno-Garcia, M. C. & Lopez-Bustins, J. A. (2020), 'Estimating barcelona's metropolitan daytime hot and cold poles using landsat-8 land surface temperature', *Science of The Total Environment* **699**, 134307.  
**URL:** <https://www.sciencedirect.com/science/article/pii/S0048969719342962>
- Li, D. & Bou-Zeid, E. (2013), 'Synergistic interactions between urban heat islands and heat waves: The impact in cities is larger than the sum of its parts', *Journal of Applied Meteorology and Climatology* **52**(9), 2051–2064.
- Ma, X., Huete, A., Tran, N. N., Bi, J., Gao, S. & Zeng, Y. (2020), 'Sun-angle effects on remote-sensing phenology observed and modelled using himawari-8', *Remote Sensing* **12**(8), 1339.
- Macarof, P. & Statescu, F. (2017), 'Comparasion of ndbi and ndvi as indicators of surface urban heat island effect in landsat 8 imagery: a case study of iasi', *Present Environment and Sustainable Development* (2), 141–150.
- Mahiny, A. S. & Turner, B. J. (2007), 'A comparison of four common atmospheric correction methods', *Photogrammetric Engineering & Remote Sensing* **73**(4), 361–368.

- Martinelli, A., Kolokotsa, D.-D. & Fiorito, F. (2020), 'Urban heat island in mediterranean coastal cities: The case of bari (italy)', *Climate* **8**(6), 79.
- Melchiorri, M., Florczyk, A. J., Freire, S., Schiavina, M., Pesaresi, M. & Kemper, T. (2018), 'Unveiling 25 years of planetary urbanization with remote sensing: Perspectives from the global human settlement layer', *Remote Sensing* **10**(5), 768.
- Nakayama, T. & Fujita, T. (2010), 'Cooling effect of water-holding pavements made of new materials on water and heat budgets in urban areas', *Landscape and Urban Planning* **96**(2), 57–67.  
**URL:** <https://www.sciencedirect.com/science/article/pii/S0169204610000344>
- Nechyba, T. J. & Walsh, R. P. (2004), 'Urban sprawl', *Journal of Economic Perspectives* **18**(4), 177–200.
- Nouri, A. S., Costa, J. P. & Matzarakis, A. (2017), 'Examining default urban-aspect-ratios and sky-view-factors to identify priorities for thermal-sensitive public space design in hot-summer mediterranean climates: The lisbon case', *Building and Environment* **126**, 442–456.
- Oke, T. R. (1982), 'The energetic basis of the urban heat island', *Quarterly Journal of the Royal Meteorological Society* **108**(455), 1–24.
- Olaode, A., Naghdy, G. & Todd, C. (2014), 'Unsupervised classification of images: A review', *International Journal of Image Processing* **8**, 2014–325.
- Pacione, M. (2009), *U Ban Geography: A Global Perspective*, Routledge.
- Pérez-Planells, L., Niclòs, R., Puchades, J., Coll, C., Götsche, F.-M., Valiente, J. A., Valor, E. & Galve, J. M. (2021), 'Validation of sentinel-3 slstr land surface temperature retrieved by the operational product and comparison with explicitly emissivity-dependent algorithms', *Remote Sensing* **13**(11), 2228.

- Ramamurthy, P. & Bou-Zeid, E. (2017), 'Heatwaves and urban heat islands: a comparative analysis of multiple cities', *Journal of Geophysical Research: Atmospheres* **122**(1), 168–178.
- Roth, M., Oke, T. R. & Emery, W. J. (1989), 'Satellite-derived urban heat islands from three coastal cities and the utilization of such data in urban climatology', *International Journal of Remote Sensing* **10**, 1699–1720.
- Salvati, A., Roura, H. C. & Cecere, C. (2017), 'Assessing the urban heat island and its energy impact on residential buildings in mediterranean climate: Barcelona case study', *Energy and Buildings* **146**, 38–54.
- Santamouris, M. (2013), *Energy and climate in the urban built environment*, Routledge.
- Schowengerdt, R. (1997), 'Thematic classification', *Remote Sensing: Models and Methods for Image Processing. 2nd ed. San Diego, CA: Academic* pp. 457–451.
- Sekertekin, A. (2019), 'Validation of physical radiative transfer equation-based land surface temperature using landsat 8 satellite imagery and surfrad in-situ measurements', *Journal of Atmospheric and Solar-Terrestrial Physics* **196**, 105161.
- Sobrino, J. A. & Irakulis, I. (2020), 'A methodology for comparing the surface urban heat island in selected urban agglomerations around the world from sentinel-3 slstr data', *Remote Sensing* **12**(12), 2052.
- Stewart, I. D., Oke, T. R. & Krayenhoff, E. S. (2014), 'Evaluation of the 'local climate zone'scheme using temperature observations and model simulations', *International journal of climatology* **34**(4), 1062–1080.
- Stone, B., Hess, J. J. & Frumkin, H. (2010), 'Urban form and extreme heat events: Are sprawling cities more vulnerable to climate change than compact cities?', *Environmental Health Perspectives* **118**(10), 1425–1428.



- Stone Jr, B. & Rodgers, M. O. (2001), 'Urban form and thermal efficiency: how the design of cities influences the urban heat island effect', *American Planning Association. Journal of the American Planning Association* **67**(2), 186.
- Tan, K. C., Lim, H. S., Mat Jafri, M. Z. & Abdullah, K. (2009), 'Landsat data to evaluate urban expansion and determine land use/land cover changes in penang island, malaysia', *Environmental Earth Sciences* **60**, 1509–1521.
- Tarng, W., Ou, K.-L., Lu, Y.-C., Shih, Y.-S. & Liou, H.-H. (2018), 'A sun path observation system based on augment reality and mobile learning', *Mobile Information Systems* **2018**.
- Torrens, P. (2008), 'A toolkit for measuring sprawl', *Applied Spatial Analysis and Policy* **1**, 5–36.
- Tyagi, P. & Bhosle, U. (2014), 'Radiometric correction of multispectral images using radon transform', *Journal of the Indian Society of Remote Sensing* **42**(1), 23–34.
- Valor, E. & Caselles, V. (1996), 'Mapping land surface emissivity from ndvi: Application to european, african, and south american areas', *Remote sensing of Environment* **57**(3), 167–184.
- Wan, Z. & Dozier, J. (1996), 'A generalized split-window algorithm for retrieving land-surface temperature from space', *IEEE Transactions on geoscience and remote sensing* **34**(4), 892–905.
- Yamamoto, Y. (2006), Measures to mitigate urban heat islands, Technical report, NISTEP Science & Technology Foresight Center.
- Yang, C., Wang, R., Zhang, S., Ji, C. & Fu, X. (2019), 'Characterizing the hourly variation of urban heat islands in a snowy climate city during summer', *International Journal of Environmental Research and Public Health* **16**(14).  
**URL:** <https://www.mdpi.com/1660-4601/16/14/2467>

- Yang, C., Yan, F. & Zhang, S. (2020), ‘Comparison of land surface and air temperatures for quantifying summer and winter urban heat island in a snow climate city’, *Journal of Environmental Management* **265**, 110563.  
**URL:** <https://www.sciencedirect.com/science/article/pii/S0301479720304965>
- Yang, L., Qiana, F., Song, D.-X. & Zheng, K.-J. (2016), ‘Research on urban heat-island effect’, *Procedia Engineering* pp. 11–18.
- Yu, X., Guo, X. & Wu, Z. (2014), ‘Land surface temperature retrieval from landsat 8 tirs—comparison between radiative transfer equation-based method, split window algorithm and single channel method’, *Remote sensing* **6**(10), 9829–9852.
- Yu, X., Yan, Q. & Liu, Z. (2010), Atmospheric correction of hj-1a multi-spectral and hyper-spectral images, in ‘2010 3rd International Congress on Image and Signal Processing’, Vol. 5, IEEE, pp. 2125–2129.
- Zerafa, S. (2020), ‘Measuring the loss of arable and rural lands on the maltese islands through satellite images’.
- Zhan, W., Chen, Y., Zhou, J., Wang, J., Liu, W., Voogt, J., Zhu, X., Quan, J. & Li, J. (2013), ‘Disaggregation of remotely sensed land surface temperature: Literature survey, taxonomy, issues, and caveats’, *Remote Sensing of Environment* **131**, 119–139.